Università degli Studi di Milano

GRADUATE SCHOOL OF VETERINARY SCIENCES
FOR ANIMAL HEALTH AND FOOD SAFETY
<u>Director:</u> Prof. Valentino Bontempo

Doctoral Program in Veterinary Clinical Sciences

Academic Year: 2013-2014

High field magnetic resonance and multidetector computed tomography of the normal canine stifle under varying flexion angles

Silvia Marches

Tutor:

Prof. Mauro Di Giancamillo

Coordinator:

Prof. Fausto Cremonesi

Index

CHAPTER 1

Foreword

1. Foreword

The canine stifle joint represents a diagnostic challenge because of its complex composition.

Knowledge of the normal anatomy of the stifle joint is essential for make full use of and interpret the information given by these modern imaging technologies. The lack of familiarity with the normal cross-sectional anatomy is a major factor slowing the learning process for interpreting CT and MR images; therefor the cross-sectional anatomy has to be studied and the easiest way to learn is directly from it. Normal canine stifle MRI anatomy is available (Baird et al., 1998; Pujol et al., 2010) and several comparative studies between different modalities are present (Samii et al., 2003; Soler et al., 2007; D'Anjou et al., 2008). However to our knowledge no studies were performed both with high field MRI and multislice CT on stifles of dogs positioned in different flexion angles.

Positioning is an important factor to improve observation of the intraarticular structures. In human medicine examining the knee in an achievable flexed position in daily practice is strongly recommended (Niitsu et al., 1998). Performing MR imaging with the knee in a flexed position (averaging 45° of flexion), more clearly delineated normal and torn anterior cruciate ligaments (ACLs) compared with MR imaging of the knee in an extended position (Niitsu et al., 1996).

In contrast to humans, in veterinary medicine little is known about the best positioning to perform stifle imaging.

Some authors have positioned dogs in dorsal recumbency with the pelvic limb extended (Banfield and Morrison, 2000; Soler et al. 2007) or 45° flexed (Baird et al., 1998); whereas others have used lateral recumbency (Blond et al., 2008) with the stifle in 145° of flexion (Pujol et al., 2010). To our knowledge only one study from Podadera et al. (2014) evaluated the effects of stifle positioning and scan plane on the visualization of the cranial cruciate ligament, using low-field magnetic resonance imaging. Stifles were imaged in three different angles (90°-135°-145°). Findings supported the use of a 90° flexed stifle position for maximizing visualization of the cranial cruciate ligaments.

1.1 Functional anatomy of the stifle joint

The stifle (*articulatio genus*) is a complex, condylar, synovial joint that allows motion in three planes (Carpenter and Cooper, 2000).

It's composed of two strictly in-built parts: the femorotibial (*articulatio femorotibialis*) and the femoropatellar articulation (*articulatio femoropatellaris*) (Barone 2004).

The movement of the femur relative to the tibia can be described by a set of three mutual orthogonal axes (x, y and z) (Fig. 1). The x axis passes through the femoral condyles parallel to the joint line in a medial-lateral direction. The y axis is parallel to the shaft of the tibia and passes through the medial tibial condyle just medial to the center of the tibial plateau. The z axis passes through the center of the joint space in a craniocaudal orientation.
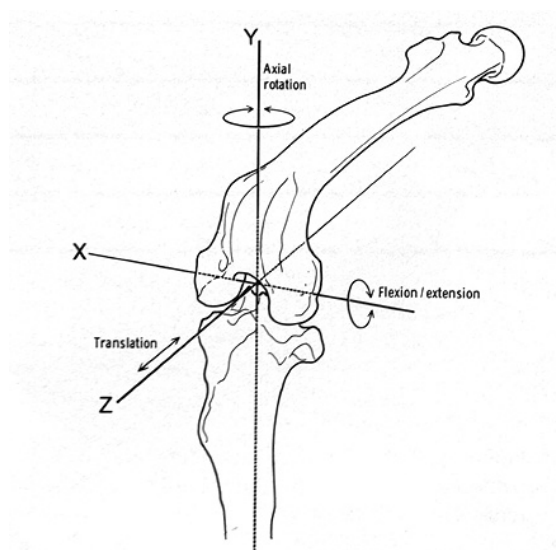
Fig. 1 - Schematic drawing of the stifle joint of the dog shows the three axes of motion (x, y and z) and their orientation.

Rotation about each axis, as well as sliding along each axis, results in six basic movements of the stifle joint (six degrees of freedom).

The primary motion of the joint is flexion and extension. However, as the femoral condyles roll and slide on the tibial table, there is cranial and caudal displacement, compression and distraction, internal and external rotation, varus and valgus angulation, and lateral and medial translation (Arnoczky et al., 1977; Korvick et al., 1994).

In a normal stifle there is a combined motion in two planes. Flexion and extension take place about the x axis, while rotatory movement of the tibia on the femur occurs about the y axys (Arnoczky, 2001).

The complexity of all these motions is directly related to the structure and functions of the anatomical components that form the joint: the condylar portion of the distal femur, proximal tibia, and proximal fibula, as well as the pelvic limbs muscles, joint capsule, joint ligaments, and menisci (Carpenter and Cooper, 2000; Robins, 1990).

Alteration in one of these components can leads to dysfunction of the joint as well as an increased risk of damage of the other structures. Therefore understanding of the normal anatomy of the stifle joint is essential for proper diagnosis and treatment (Carpenter and Cooper, 2000).

The main spheroidal part of the stifle joint is formed by the thick, rollerlike condyles of the femur articulating with the flattened condyles of the tibia to form the femorotibial or condyloid part of the joint. Between the trochlea of the femur and the patella there is the femoropatellar joint. The two joints are in interdependent and they work complementary: the patella is held to the tibia firmly by ligamentous tissue so that any movement between the femur and the tibia also occurs between the patella and the femur (Evans and de Lahunta, 2013). For this reason it's preferable to consider them as one composed synovial joint (Barone, 2004).

1.1.1 The menisci

The incongruence that exist between the tibia and the femur is occupied by two biconcave C-shaped fibrocartilagenous discs, the menisci, one located between the adjacent medial condyles (*meniscus medialis*), and the other (*meniscus lateralis*) between the adjacent lateral condyles of the femur and tibia (Carpenter and Cooper, 2000; Evans and de Lahunta, 2013).

They have sharp, deeply concave axial, and thick convex abaxial borders (Evans and de Lahunta, 2013). On cross-section the menisci are wedge-shaped (Robins, 1990). The lateral meniscus is slightly larger and thicker than the medial (Robins, 1990; Arnoczky, 2001, Evans and de Lahunta, 2013).

In man the menisci have been shown to have the major functions of load bearing and load distribution. They are also responsible for shock absorption (Bellenger, 1995; Messner and Gao, 1998). In the dog, they also deepen the tibial articular surface and provide better accommodation of the femoral condyles on the tibial plateau. They increase the stability of the joint during the flexion-extension and rotatory movements and relieve the incongruence between the femur and the tibia (Robins, 1990; Carpenter and Cooper, 2000; Arnoczky, 2001).

Joint motion results in motion of the menisci, therefore they are considered dynamic structures. During flexion the menisci slides caudally on the tibial plateau. However, the medial meniscus slides much less than the lateral because of its attachment to the medial collateral ligament and joint capsule (Carpenter and Cooper, 2000; Arnoczky, 2001) (Fig. 2). The caudal displacement of the lateral femoral condyle on the tibia during flexion makes the caudal displacement of the lateral meniscus even more pronounced and, in extreme flexion, it may protrude over the edge of the tibial plateau. During extension both menisci slide cranially on the tibial plateau.

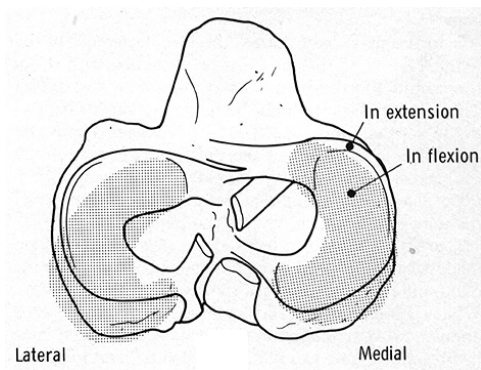Fig. 2- Dorsal aspect of the tibia. Normal excursion of the menisci in extension and flexion (shaded) (Mod. Arnoczky et al., 1977).

1.1.2 Stifle joint ligaments

Meniscal ligaments

The meniscal ligaments attach the menisci to the tibia and femur.
The **cranial tibial ligament of the medial meniscus** goes from the cranial, axial angle of the medial meniscus to the cranial intercondyloid area of the tibia,

immediately cranial to the transverse ligament, the cranial tibial attachment of the lateral meniscus, and the tibial attachment of the cranial cruciate ligament.

The **caudal tibial ligament of the medial meniscus** goes from the caudal axial angle of the medial meniscus to the caudal intercondyloid area of the tibia, just cranial to the tibial attachment of the caudal cruciate ligament.

The **cranial tibial ligament of the lateral meniscus** goes to the cranial intercodyloid area of the tibia, where it attaches caudal to the transverse ligament and the cranial tibial attachment of the medial meniscus.

The **caudal tibial ligament of the lateral meniscus** goes from the caudal axial angle of the lateral meniscus to the popliteal notch of the tibia just caudal to the caudal intercodyloid of the tibia.

The **femoral ligament of the lateral meniscus** (*lig. meniscofemorale*) is the only femoral attachment of the menisci. It goes from the caudal axial angle of the lateral meniscus dorsally to that part of the medial femoral condyle that faces the intercondyloid fossa.

The **transverse ligament** (*lig. transversum genus*) is a small transverse fibrous band that goes from the caudal side of the cranial tibial ligament of the medial meniscus to the cranial part of the cranial tibial ligament of the lateral meniscus (Evans and de Lahunta, 2013).

Femorotibial ligaments

The femorotibial ligaments are the collateral and the cruciate ligaments.

The cruciate ligaments are intraarticular and they are covered by synovial membrane. The **cranial cruciate ligament** (*lig. cruciatum craniale*, CrCL) runs from the caudomedial part of the lateral condyle of the femur across the intercodyloid fossa to the cranial intercondyloid area of the tibia (Evans and de Lahunta, 2013).

The **caudal cruciate ligament** (*lig. cruciatum caudale*, CdCL) is slightly thicker and longer than the cranial one and runs from the lateral surface of the medial femoral condyle caudo-distally to the lateral edge of the popliteal notch of the tibia.

As their name implies, the cruciate ligaments cross each other in their proximal ends in the intercondylar fossa.

The cruciate ligaments function as joint movement regulators.

Functionally each cruciate ligament has two bands. The CrCL has a caudolateral band that is taut in extension and relaxed in flexion, and a craniomedial band that is taut both in flexion and in extension.

The CdCL has a cranial band that is taut in flexion and relaxed in extension (Arnoczky and Marshall, 1977).

For their anatomical relations, the cruciate ligaments begin to twist one on another as the stifle flexes and the tibia internal rotates on the femur (Arnoczky, 2001). This twisting action limits the amount of normal rotation of the tibia. The rupture of both the cruciates causes an anomalous increase in this internal rotation of the tibia (Arnoczky and Marshall, 1977).

As the stifle extends, the cruciate ligaments "untwist", so they have no control on external rotation. An excessive external rotation, associated with cruciate ligament, is present only when there is a concurrent collateral ligament rupture (Arnoczky and Marshall, 1977).

The CrCL also functions to prevent cranial displacement of the tibia in relation to femur, limit excessive internal rotation of the tibia, by twisting on CdCl, and prevent hyperextension of the stifle. The CdCL functions to prevent caudal displacement of the tibia in relation to the femur and to limit excessive internal rotation of the tibia in conjunction with the CcCL (Arnoczky and Marshall, 1977; Arnoczky, 1988).

The collateral ligaments develop in the fibrous layer of the joint capsule.

The **medial collateral ligament** (*lig. collaterale mediale*, MCL) is a thick ligament that originates from the medial femoral epicodyle, extends distally, forms a strong attachment with the joint capsule and the medial meniscus and inserts on the proximal medial region of the tibia (Carpenter and Cooper, 2000). There is a fluid-filled bursa located between the ligament and the tibia that reduces friction and aids the movement of the MCL caudally during flexion of the joint (Vasseur and Arnoczky, 1981).

The **lateral collateral ligament** (*lig. collaterale laterale*, LCL) originates in the area of the lateral femoropatellar ligament and, as it crosses the joint cavity, it passes over the tendon of origin of the popliteus muscle. It ends distally on the head of the fibula, with a few fibers going to the adjacent lateral condyle of the tibia (Evans and de Lahunta, 2013).

Vasseur and Arnoczky (1981) studied the anatomic features and functions of the collateral ligaments. They found that the collateral ligaments work together with

the cruciates to provide rotational stability of the joint both in flexion and extension (Fig. 3 A, B).

In extension the collateral ligaments are stretched and provide the primary check against internal rotation with the cruciate ligaments acting as a secondary restraint (Vasseur and Arnoczky, 1981). During flexion the LCL loosens and this loosening combined with the less rigid attachment of the lateral meniscus, allows internal rotation of the tibia relative to the femur (Vasseur and Arnoczky, 1981; Slocum and Devine, 1983). In the intact stifle the internal rotation is checked by the twisting of the cruciates on one another. Thus, the cruciate ligamets provide the primary check against internal rotation of the tibia during flexion (Vasseur and Arnoczky, 1981; Arnoczky, 1988). Lateral rotation is limited only by the collaterals, both in flexion and extension.
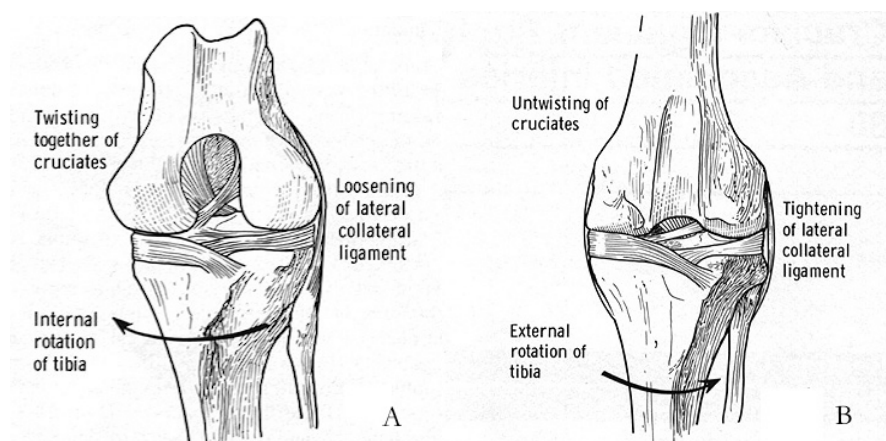
Fig. 3 - A: during flexion the lateral collateral ligament loosens allowing internal rotation of the tibia on the femur. The cruciate ligaments "twist" on each other to limit this internal rotation. B: during extension the lateral collateral ligament tightens and the tibia rotates externally. The cruciate ligaments "untwist" and thus have no effect on limiting external rotation (mod. Arnoczky et al., 1977)

Patellar ligaments

The **patellar ligament** (*lig. patellae*) is the portion of the tendon of the muscle quadriceps femoris from the patella, intercalated in the tendon, to the tibial tuberosity. It's separated from the synovial membrane of the joint capsule by a large quantity of fat (Evans and de Lahunta, 2013).

The patella is held in the trochlea of the femur mainly by the thick lateral femoral fascia, or fascia lata, and the thinner medial femoral fascia (Evans and de Lahunta, 2013).

The delicate **medial and lateral femoropatellar ligaments** (*ligg. femoropatellare mediale et laterale*) run from the patella to the fabellae and merge with the femoral fascia and function weakly to hold the patella in the trochlea (Robins 1990, Evans and de Lahunta, 2013).

1.1.3 The joint capsule

The canine stifle joint capsule is the largest in the body. It is composed of two layers and forms three intercommunicating sacs (Carpenter and Cooper, 2000). Two of these are between the femoral and the tibial condyles (*saccus medialis and lateralis*) and the third between the patella and the trochlea of the femur (Evans and de Lahunta, 2013).

The outer layer of the capsule, the fibrous layer, is composed of dense, inelastic, fibrous connective tissue. The inner layer or synovial membrane is a specialized, vascular, connective tissue that produces synoial fluid, contains the nerve supply and produces phagocytic synoviocytes (Leeson et al., 1988). The two layers are in close contact except distally at the apex of the patella where they are separated by the **infrapatellar fat body** (*corpus adiposum infrapatellare*) (Leeson et al., 1988; Evans and de Lahunta, 2013).

The normal canine stifle contains 0.2 to 2 ml of a transparent, viscous fluid that is primarily composed of water and a strongly polymerized hyaluronic acid (Leeson et al., 1988; Evans and de Lahunta, 2013). The synovial fluid serves as a lubricant and additionally it supplies nutrients to, and removes metabolites from, the avascular articular cartilage and menisci (Leeson et al., 1998; Carpenter and Cooper, 2000).

1.2 Diagnostic imaging of the stifle joint

The canine stifle joint represents a diagnostic challenge because of its complex composition: it's an arrangement of osseous, articular, fibrocartilaginous and ligamentous structures (Marino and Loughin 2010) and is one of the most frequently injured joints in dogs (Vasseur 1993; Johnson et al. 1994; Gielen et al., 2010).

Traumatic or degenerative changes are frequently seen, with meniscal and cranial cruciate ligament (CrCL) lesions most commonly diagnosed (Rose et al., 2011). The small size of stifle joint structures, the restricted joint space and its intricate composition make diagnostic imaging a challenge. Diagnosis of stifle disease is based on a history of lameness, physical exam findings (Reed et al., 1995; Kramer et al., 1999; Soler et al., 2007) and radiography remains the most important initial diagnostic step (Marino and Loughin, 2010). The presence of different tissue types and their superimposition limit successful diagnostic imaging with a single modality (Marino and Loughin, 2010). More recently several advanced imaging modalities have been employed to image the canine stifle.

Progress in computing technology has accelerated advances in diagnostic imaging. The key to successful management of the diagnostic options is to recognize the strengths and weaknesses of each modality and to use a multimodality approach, to provide a complete assessment of complex structures.

1.2.1 Arthroscopy

In obscure case of knee injury in human orthopaedics, arthroscopic investigation, following careful physical examination, is a direct standard diagnostic procedure and a valuable tool to determine the possible treatment (Noyes et al. 1980, 1989; Odensten et al. 1985). Arthroscopy of the canine stifle joint allows direct visualization and careful probing to reveal minor surface fraying or subsynovial tears (Kivumbi and Bennet, 1981; Miller and Presnell, 1985; Van Ryssen, 1996). The visible structures are the cruciate ligaments, the menisci, the intercodyloid fossa, the patella, the femoral condyles and the tibial plateau (Tomlinson, 2006). However, complete evaluation of the menisci is impossible because of anatomic constraints. The tibial surface remains hidden

from view, as does the integrity of internal meniscal structures (Flo 1993). Additional surgery after surgical stabilization for cranial cruciate ligament lesion may be neede for undiagnosed meniscal pathology (Metelman et al., 1995). The drawback to arthrography is its invasiveness and therefore the need for anesthesia. In addition, the basic equipment needed to perform arthroscopy is not widely spread in veterinary practice and it requires experience. Alternative diagnostic approach to arthroscopy has been investigated.

1.2.2 Radiography

The acquisition of extremity radiographs is one of the most common radiographic examinations performed in Veterinary Medicine practice (Thrall, 2013). Radiography is the most used technique for orthopedic conditions and remains the most important initial step (Marino and Loughin, 2010).
Radiography is ideal for stifle orthopedic conditions for its properties of energy absorption: tissues do not absorb X-rays uniformly and soft tissues absorb fewer than bone resulting in images that are shades of gray whereas bone appears radiopaque (Thrall, 2013).
Obtaining good-quality radiographs of extremities is easier than other body regions because the parts are thinner and can be positioned more easily (Thrall, 2013).

Radiographic examination of the appendicular system should consist of minimum of two orthogonal projections, a lateral view and a craniocaudal view. The primary X-ray beam should be centered on the joint.
Most of the abnormalities are seen on standard radiographic views, but stress view may be necessary to solidify the diagnosis (De Rooster et al., 1998; De Rooster and Van Bree, 1999, Marino and Loughin, 2010).

Radiographic evidence of disease may include: compression of the infrapatellar fat pad, increased synovial fluid volume or thickening of the synovial lining, altered joint space, decreased or increased subchondral bone opacity, mineralization of soft tissues, intraarticular mineralization, joint displacement, or joint malformation (Thrall, 2013).
Evaluation of subchondral bone, articular margins, and regions of ligament, tendon, and joint capsule attachment are easily assessed with conventional

radiology (Carrig, 1997). The most common pathological conditions that can be indirectly diagnosed with radiography are osteoarthritis (OA), cranial cruciate ligament (CCL) rupture, osteochondrosis, arthritis and neoplasia. Changes noted with stifle osteoarthritis are narrowing of the joint space, subchondral sclerosis of the tibial plateau, cystic lesions, intraarticular mineralization, bone remodeling, and joint capsule distension identified as proximal displacement of the infrapatellar fat pad and caudal displacement of the capsule (Marino and Loughin, 2010).

Cranial cruciate ligament (CCL) rupture is characterized by intraarticular swelling, cranial displacement of the tibia and, in chronic cases, OA changes.

Osteochondrosis is a disruption of osteochondral ossification resulting in cartilagineous lesions with sclerotic margins, commonly involving the medial and lateral condyle, osteochondral fragments, and secondary OA (Kippenes and Johnston, 1998).

Radiographs of arthritis, infectious or noninfectious, may only reveal soft tissue swelling in the early stages, subchondral bone erosion and sclerosis, narrowing of the joint space, and signs of OA in more advanced cases

Neoplasia of the stifle is uncommon and synovial sarcoma is the most common type observed. Soft tissue swelling and periosteal proliferation, with multifocal areas of bone destruction in periarticular locations, extending into articular regions with possible bone involvement, are the characteristics signs.

For most diseases of the stifle, radiography may be sometimes sufficient to make a diagnosis. However, for its difficult in evaluating soft tissues, more advanced imaging may be necessary.

In addition, we need to consider patient and operator exposition to radiations. Sedation is needed but short acquisition time.

Radiographs with added contrast medium (air or water-soluble iodinated contrast medium) can be used to enhance visualization of intraarticular structures, such as the synovium and the cartilage (Thrall, 2013). However, arthrography routinely use is not justified (Hay et al., 1996) and it has been largely replaced by computed tomography and magnetic resonance imaging.

1.2.3 Ultrasonography

Ultrasonography (US) is a safe, non-invasive, relatively low cost additional diagnostic tool to clinical and radiological examination: radiology can evaluate the bony aspects of the joint and their relationship to each other, sonography allows visualization of the soft tissue (Kramer et al. 1999).

The ability of ultrasonography (US) to image intra-articular soft-tissue structures and to provide additional information, which can be used in conjunction with radiography, has been reported by several authors (Kramer et Gerwing, 1996; Soler et al). Furthermore, US has been proven to be useful to evaluate musculoskeletal soft tissues that are not visible radiographically (Reed et al., 1995; Kramer et al., 1999; Gnudi and Bertoni, 2001; Arnault et al., 2009).

Sound waves travel fastest through bone and slower in joint fluid, making ultrasonography more useful for soft tissue structures of the stifle. However ultrasound images generally have low resolution and soft tissue contrast (Fitch et al., 1997).

In a study from Gnudi and Bertoni (2001) sonography was not an accurate test for cruciate ligament rupture evaluation in dogs, identifying only 20% of ruptured cruciate ligaments. Although not an incisive diagnostic procedure for this condition, it was specific for the soft tissue pathologic changes which were observed consequent to joint stability.

Ultrasound has been reported to be a reliable technique for identification of osteochondrosis lesions in the lateral femoral condyle. The menisci are less reliably imaged in small dogs, but cranial cruciate ligament and femoral articular cartilage can be seen.

Type and biologic behavior of tumors cannot be assessed using ultrasound, but it can demonstrate the extent of soft tissue involvement (Kramer et al. 1999; Marino and Loughin, 2010).

However there are several major limitations to the routine use of ultrasound in evaluating the stifle. Individual US images represent only a portion of the complete cross-sectional anatomy of the region. Furthermore, the US beam is unable to penetrate structures that contain mineral and, in small and medium breed dogs, the joint space is too narrow, resulting in a limited window for image production (Kramer et al., 1999).

Complete evaluation of the menisci is difficult. Normally the meniscus is inhomogeneous and congruent with the margins of the femoral and tibial

condyles (Marino and Loughin, 2010). The meniscal ligaments, intermeniscal ligaments, collateral ligaments and synovia cannot be differentiated (Reed et al., 1995; Kramer, 1999).

Ultrasound images generally have low resolution and soft tissue contrast and its operator dependence may make other modalities more useful (Marino and Loughin, 2010).

1.2.4 Computed tomography

Computed tomography (CT) is based on tomography technology, which allowed for an image of a single slice of the body to be produced on radiographic film (Marino and Loughin, 2010). In contrast to radiography, where there is summation of overlying structures, cross-sectional imaging allows improved resolution of anatomic structures (Samii and Dyce, 2004).

Images can be manipulated, with a computerized process know as windowing, to reveal various structures based on tissue characteristics (Marino and Loughin, 2010). Modern scanners allow this data to be reformatted as volumetric (3D) representations of structures and a 3D model can be constructed, displayed and manipulated for presurgical planning.

Computed tomography (CT) is very sensitive in demonstrating calcified or bony structures and also allows evaluation of the soft-tissues using appropriate windows (Samii and Dyce, 2004; Soler et al., 2007; Samii et al., 2009; Gielen et al., 2010). The osseous structures and the infrapatellar fat pad are clearly identifiable (Samii, 2011).

With cruciate ligament and meniscal cartilage tears joint capsular thickening and intracapsular effusion is always seen, periarticular degenerative osseous changes are often present, small osseous bodies (osteochondromas or avulsion fragments) may be seen. Reformation of the acquired transverse or frontal planar images is necessary to fully assess the cruciate and meniscal structures and intra-articular contrast medium is necessary to clearly see the intra-articular soft tissue structures (Samii, 2011).

Multislice CT allows very quick scanning of the patient. However general anesthesia required. The development of safe, short-term anesthetic protocols will play a major role for the full implementation of multislice CT in veterinary practice.

In addition, even if CT scanners have the benefit to of providing better osseous visualization and shorter scan times when compared with MRI, most stifle imaging studies in veterinary medicine are centered on intraarticular ligamentous abnormalities, making MRI a more suitable modality.

1.2.5 Magnetic resonance imaging

Magnetic resonance imaging (MRI) is currently one of the most effective diagnostic tools for assessment of joint disorders and has led to a better understanding of normal anatomy and pathologic features in people (Grainger et al., 2000). The major advantages of MRI are its excellent image resolution, superior soft tissue contrast, the possibility to image in multiple planes and use of a magnetic field rather than ionizing radiations. All of these features have made MRI the diagnostic modality of choice for traumatic, degenerative and inflammatory diseases of joints in people (Rubin et al., 2000). Moreover, it is also the only noninvasive modality that allows combined evaluation of articular cartilage, subchondral bone and soft tissue structures associated with the joint. For all these reasons MRI of the knee is reported to be the most common non-neurologic application in human medicine (Chan et al., 1994).

From the first description of MRI of the canine stifle in 1991 (Widmer et al. 1991), several studies have described the use of low- and high- field MRI for the detection of intraarticular lesions and for diagnostic investigation of stifle injuries and degenerative changes (Baird et al., 1998; Martig et al, 2006; Blond et al., 2008; D'Anjou et al., 2008). MRI may allow non-invasive confirmation of tendon, as well as associated muscle injury, prior to typical chronic changes (Fitch et al., 1997) and it has become the preferred imaging modality for the evaluation of the articular cartilage, menisci and ligaments of synovial joints (Widmer et al., 1994) also in Veterinary Medicine.

Magnetic resonance imaging (MRI) offers a greater ability to directly and non-invasively assess joint morphology and discriminate all articular tissues, including bone, synovium, and cartilage (D'Anjou et al., 2008). In particular high-field MRI has been described to be more sensitive than computed radiography in assessing onset and progression of degenerative changes in canine experimental osteoarthritis and to provide discrimination between joint effusion and synovial thickening (D'Anjou et al., 2008).

New sequences and improved techniques for canine stifle MR imaging have been described (Baird et al., 1998; Soler et al., 2007; Pujol et al., 2011; Podadera et al., 2014).

Baird et al. described the utility of MRI in imaging the structures of the stifle joint using a low field MRI in sagittal and dorsal plane. Another study by Soler compared the effectiveness of US, CT and MRI in imaging the different structures of the stifle in plastinated cross-sectional slices of cadaver specimens and used these images to create an atlas of normal anatomy. Pujol et al. compared low-field MRI and MR arthrography in normal canine stifles to gross dissection. They showed that, with the exception of poor delineation of articular cartilage, both protocols provide images of adequate quality to assess the normal canine stifle joint. All of these studies were performed positioning the stifle in a single flexion angle. Podadera et al. evaluated the stifle joint at three different flexion angles using low-field MR, comparing the visualization of the cranial cruciate ligament. MR images of the stifle at a 90° angle resulted in better visualization of the cranial cruciate ligament.

However, MRI is an expensive diagnostic tool, limited in availability to clinical veterinary practice and requires general anesthesia to limit motion.

CHAPTER 2

Objectives

2. Objectives

The aim of this study was to describe and compare high-field MRI to CT anatomy of the normal canine stifle and to compare the different visualization of the main articular structures that compose stifle when it is in four different flexion angles (85°-110°-135°-160°). We focused on the cruciate ligaments, the menisci and the articular cartilage.

Performing stifle imaging at different flexion angles can be useful to better visualize the clinically most relevant structures and a valid technique for improving diagnostic accuracy. We hypothesized that stifle flexion would result in better visualization and delineation the cruciate ligaments, the menisci and the articular cartilage.

CHAPTER 3

Materials and methods

3. Materials and Methods

3.1 Specimens

The study was approved by the Institutional Animal Care and Use Committee. Six cadavers of adult dogs were collected within 12 hours of death following euthanasia for reasons unrelated to this study. Dogs were of various breeds, but were similar in size and body weight (20 - 30 kg). Palpation of each limb and orthogonal radiographs of the stifle joint were taken to rule out joint pathology. The cadavers were stored at -20° until testing.

3.2 Limb Preparation

From each dog either the right or the left stifle was randomly selected. After thawing, the limbs selected for inclusion were disarticulated at the level of the coxofemoral joints. The hair was clipped from the mid-diaphysis of the femur to the mid-diaphysis of the tibia. Two 3.5 mm tibial tunnels were drilled. These tunnels were used to provide tibial reference lines for the orientation of the MR and CT scanning enabling consistent planning of the sagittal and dorsal MR and CT image planes between the different flexion angles and between the two modalities (Tremolada et al., 2014). To allow for consistent position of the tibial tunnels, 2 Kirschner wires were placed with fluoroscopic guidance and were used as guide wires for drilling. The first wire was inserted 10 mm distal to the tibial tuberosity, in the craniocaudal direction, parallel to the tibia plateau. The second wire was inserted in the mediolateral direction, perpendicular to the first wire. By use of the guide wires, tibial tunnels were drilled with a 3.5-mm cannulated drill bit. One tibial tunnel was made in a craniocaudal orientation parallel to the tibial plateau, which was defined on the basis of radiographic landmarks. The second tunnel was made in a mediolateral orientation perpendicular to the first tunnel. The wires were removed prior to MR imaging. Limbs were stored at -10° C until imaging was performed.

3.3 Stifle-loading jig

A Polyoxymethylene (Delrin®) custom made jig was specifically built for this and a concomitant study (Tremolada et al., 2014) (Fig. 4). The device consisted

of two adjustable boards connected with a hinge mechanism, to allow the positioning of the stifle joint at different flexion angles. The proximal board, where the femur was located, had two slots on both sides where belts were inserted to strap the thigh, securing the femur. The distal board, used for the tibia, had on its distal part two rectangular blocks, to accommodate the hock joint, and a strap to secure the distal portion of the tibia.

Both parts of the jig were extendible, making possible the use of the jig for different-sized dogs. Foam sponges were packed around the hock and around the femur to minimize possible movements and rotation.
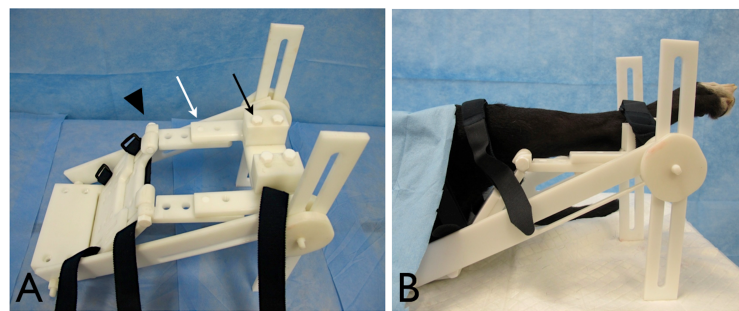
Fig. 4 **-** Custom made jig A- The central hinge (black arrowhead) positioned caudal to the stifle joint allows contol of stifle flexio. The white arrow indicates the part of the jig that allows it to fit dogs of different sizes by lengthening the jig. The black arrow indicates the portion of the jig where the tibiotarsal joint is positioned. It is possible to change the position of the 2 blocks to fit hock of different sizes. B- Pelvic limb of a dog positioned in the loading device.

3.4 Magnetic resonance imaging

Each specimen was mounted in the jig and the angle formed by tibia and femur was initially assessed was initially assessed using a plastic goniometer, aligning each arm with anatomical landmarks (lateral anatomical landmarks (lateral and medial malleolus and femur greater trochanter). Stifle joint flexion trochanter). Stifle joint flexion angle was then confirmed on mediolateral radiographs, using a radiographs, using a previously described method (Mostafa et al. 2009). The angle of the stifle joint was angle of the stifle joint was defined as the angle between the long axes of the distal portion of the distal portion of the femur and proximal portion of the tibia (

Fig. 4 – Mediolateral radiographic view of a stifle joint illustrating the measurements of the stifle joint angle. The angle (white triangle) is formed between the long axis of the distal portion of the femur and the long axis of the proximal portion of the tibia.).

A tolerance of ± 5° degrees was considered acceptable.

Following radiographs, the cadaver was positioned in a 1.5 Tesla commercial MR unit (Toshiba Titan, Toshiba America Medical Systems, Tustin, Calif.) and images were acquired using a circular surface receive-only coil.
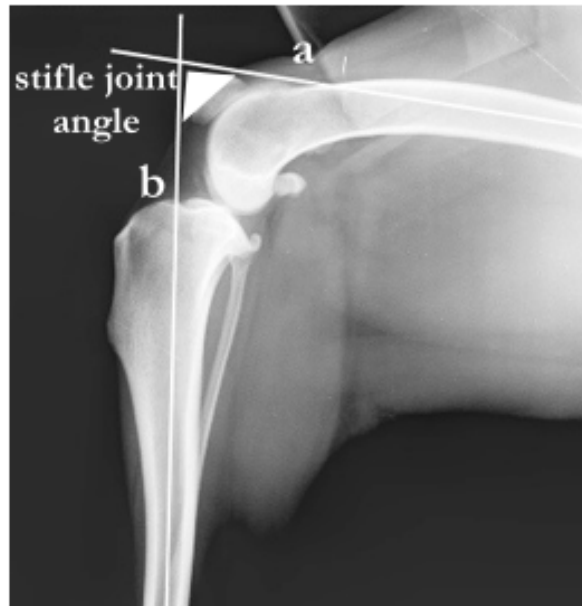
Fig. 4 – Mediolateral radiographic view of a stifle joint illustrating the measurements of the stifle joint angle. The angle (white triangle) is formed between the long axis of the distal portion of the femur and the long axis of the proximal portion of the tibia.

Localizer images were acquired in 3 planes, and the tibial tunnels were identified. Images in the sagittal plane were planned such that the image axis was perpendicular to the long axis of the mediolateral tibial tunnel and parallel to the long axis of the craniocaudal tibial tunnel. Images in the dorsal plane were planned such that the image axis was perpendicular to the long axis of the craniocaudal tibial tunnel and parallel to the long axis of the mediolateral tibial tunnel (**Fig. 5**). A proton density (PD) sequence (TR 3008, TE 18, FA 90°, ST 2 mm, matrix 304 x 320) was performed and each leg was imaged at flexion angles of 85°-110°-135°-160° degrees. All images were stored on a picture archive and communication system (PACS) in digital imaging and communications in medicine (DICOM) format.
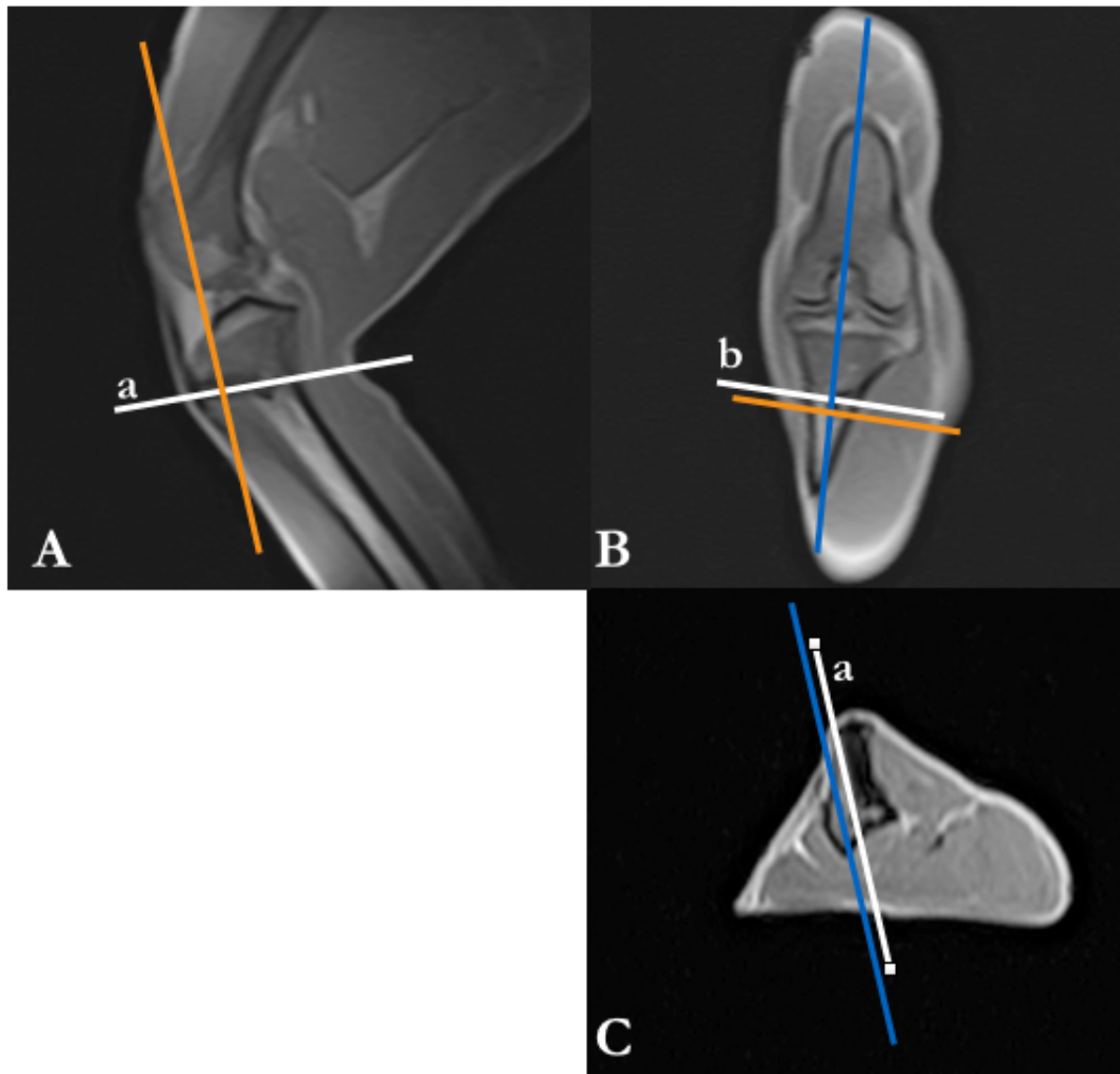
Fig. 5 – 3 planes (A: sagittal, B: dorsal, C: transverse) localizer MR images. Images in the sagittal plane were planned such that the image axis (blue line) was perpendicular to the long axis of the mediolateral tibial tunnel (b) and parallel to the long axis of the craniocaudal tibial tunnel (a). Images in the dorsal plane were planned such that the image axis (orange line) was perpendicular to the long axis of the craniocaudal tibial tunnel (a) and parallel to the long axis of the mediolateral tibial tunnel (b).

3.5 Computed tomography imaging

CT examination of each stifle joint was performed right after MRI scanning, using an 8-slices multidector CT (MDCT) scanner (Toshiba Aquilion, Toshiba America Medical Systems). Legs were positioned using a styrofoam custom jig

simulating the patient in dorsal recumbency. The angle formed by tibia and femur was initially assessed using a plastic goniometer. Then, after the acquisition of the two scout images (one lateral and one craniocaudal image, extending from the proximal femur to the tarsus) the angle was confirmed on the lateral scout image using the same method as for MR (Mostafa et al. 2009) (Fig. 5). A tolerance of ± 5° degrees was considered acceptable. Using a modified stifle protocol (100 mA, 120 KVp, 512x512 matrix, pitch 1) a data volume was obtained from the mid femoral diaphysis to the mid tibial diaphysis with contiguous 1.0-mm slice thickness and 1.0-mm slice index with a soft tissue algorithm. Each image set was reconstructed with a bone standard algorithm and volume rendered. Multiplanar reformatted images in 3 planes (sagittal, dorsal and axial) were created from the volume dataset using the aforementioned tibial tunnels as a reference. Each leg was imaged at flexion angles of 85°-110°-135°-160°. All images were stored on a picture archive and communication system (PACS) in digital imaging and communications in medicine (DICOM) format.

## 3.6 Anatomical study

After image acquisition, limbs were re-frozen (-10 °C) at 90° flexion and sagittal anatomical sections (2 mm) were obtained with a bandsaw approximately in the middle of the lateral and medial tibial condyles and intercondylar notch. When specimens were thawed, photographs at each different flexion angle were taken with a digital camera (Nikon D90). The photographs obtained from the 3 sagittal anatomical sections at each angle were matched with corresponding sagittal MRI and CT images. Relative positions of the main intra- and peri-articular structures of the stifle were compared.

3.7 Image Analysis

For each CT an MRI scan two board certified veterinary radiologists independently evaluated the cranial and the caudal cruciate ligament, the medial and the lateral meniscus, the femoral and tibial cartilage, using a visual assessment score of 0-3 and subjective criteria previously described (Podadera et al. 2014). A score of 0 indicated that the structure was not visible. A score of 1 indicated that the structure was visualized partially. A score of 2 indicated that

the totality of the structure was identified but poorly demarcated. A score of 3 indicated that the structure was totally visualized and well demarcated.

Visualization scores referred to the visibility of the joint's structures using all available CT or MRI images in one scan sequence at a specific flexion angle, both in sagittal and dorsal plane. For the CT scans the soft tissue window was evaluated (Window Level 40, Window Width 350). A MergePACS Workstation (Merge Healthcare Inc, Chicago, Ill.) was used to analyze the images. The studies were anonymized, all the data about the stifle angles removed and randomly projected.

3.8 Statistical Analysis

Statistical analysis was performed using the commercial software IBM SPSS Statistics, version 22.0 (IBM SPSS Inc., Armonk, USA).

Before any statistical test, data distribution was verified by the mean of Shapiro-Wilk test.

Visualization scores means of each parameter were tested in order to verify their distribution, since data were not normally distributed and non-parametric analysis was performed.

Visualization scores means were calculated for every structure and each angle, in both the modalities.

Using the non-parametric Wilcoxon signed-rank test the effect of the angle on the visualization scores, regardless the plane, was evaluated for each structure.

In order to find the best visualization angle for every structure a generalized estimating equation (GEE) was applied. In particular the dependent variables, since were considered as scores, were compared using a Poisson distribution and log link function was used. Goodness of fit was assessed using a quasi likelihood under independence model criterium (QIC).

A GEE was also used to evaluate the effect of the plane, regardless the flexion angle, on the visualization scores, tested for each structure in both the modalities.

Interobserver differences were tested for each modality using Wilcoxon signed-rank test. The agreement between the two observers was calculated with Kappa test using the Cohen's kappa coefficient, a statistical measure of inter-annotator agreement. The level of agreement was defined as follows: k values < 0.00

indicated no agreement; k values of 0.00-0.40 indicated a poor agreement; k values of 0.41-0.75 represented a good agreement; k values of 0.76-1.00 represented an excellent agreement.

Comparison between MRI and CT was made using a generalized estimating equation (GEE).

The threshold for statistical significance was considered to be $p < 0.05$.

CHAPTER 4

Results

4. Results

4.1 Specimens

Four male dogs and two female dogs with a mean ± SD body weight of 27 ± 5 kg were used. Two right pelvic limbs and four left pelvic limbs were used for the study.

4.2 Anatomical study

The results of the first part of this study are illustrated in the following figures (Fig. 7, **Fig. 8**, Fig. 9). The visible structures in each MRI, CT and anatomical section are indicated in the legend.

All the structures identified in the anatomical sections were visible both in CT and MRI and we were able to identify all the major stifle joint structures. Based on MRI and anatomical sections both menisci moved caudally during flexion (Fig. 7; Fig. 9). Lateral meniscal motion was greater than medial meniscus motion. During extension the cranial cruciate ligament appeared increasingly stretched and the caudal cruciate ligament relaxed (Fig. 8). Using CT images and anatomical photographs we demonstrated the caudal rolling and sliding motion of the femoral condyle during flexion (Fig. 7; Fig. 9), which matched caudal meniscal motion.
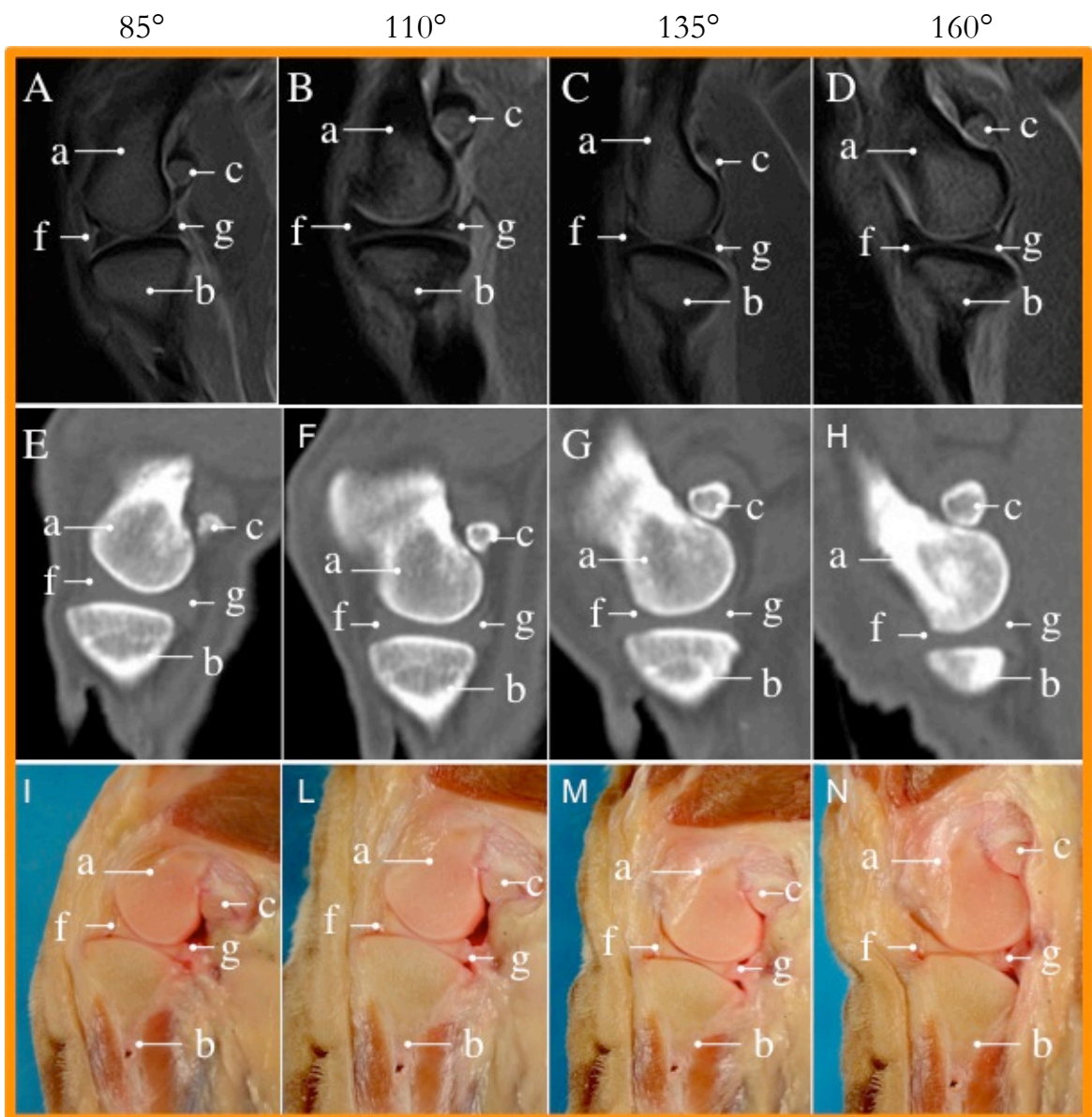
Fig. 6 – MRI (A-D), CT (E-H) and anatomical (I-N) images obtained in the middle of the medial tibial condyle at four different flexion angles. a) femur; b) tibia; c) lateral fabella; e) fibula; f) cranial horn of the medial meniscus; g) caudal horn of the medial meniscus.
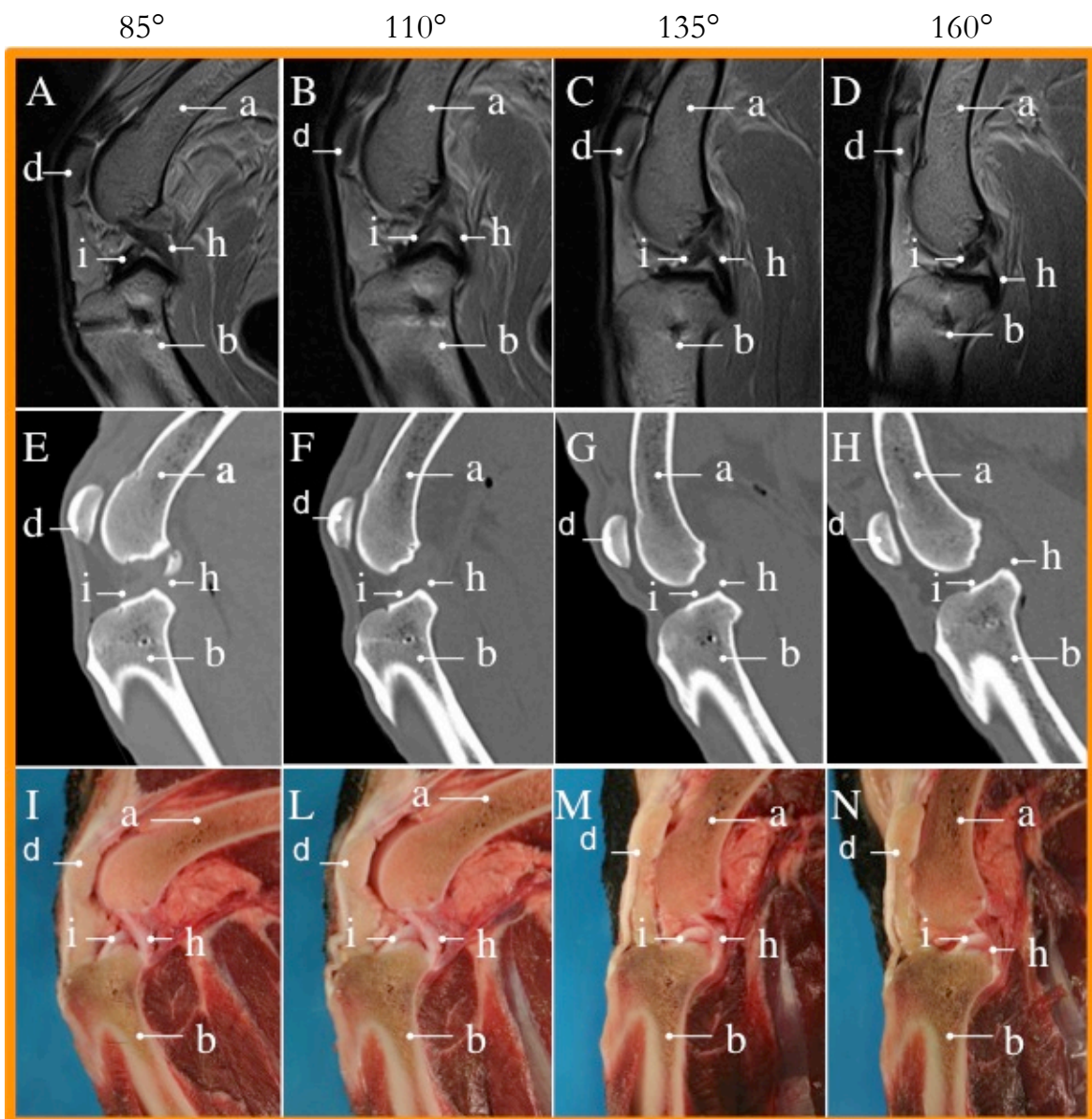
Fig. 7 - MRI (A-D), CT (E-H) and anatomical (I-N) images obtained at the level of the intercondylar notch at four different flexion angles. a) femur; b) tibia; d) patella; h) caudal cruciate ligament; i) cranial cruciate ligament.
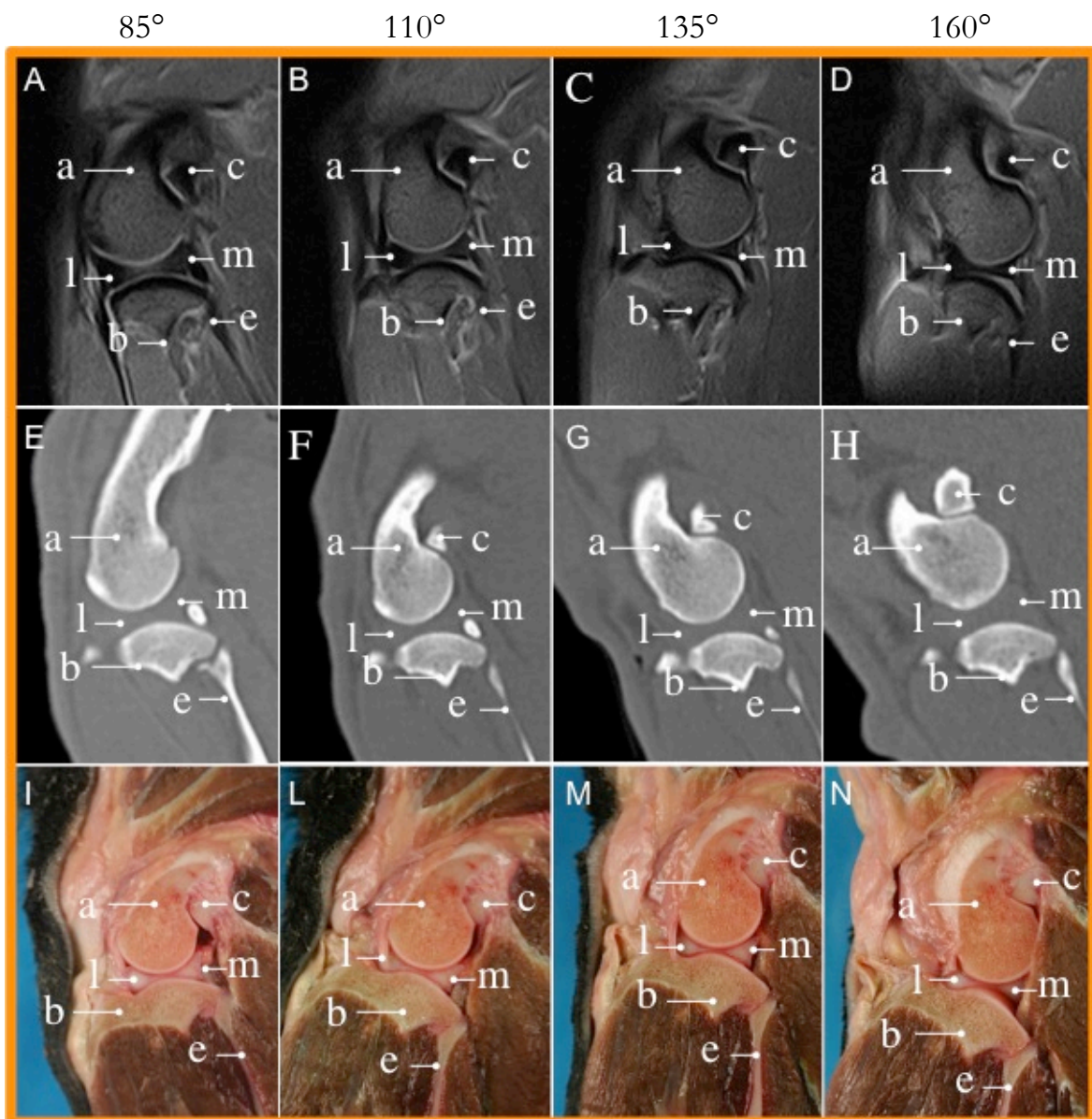
Fig. 8 - MRI (A-D), CT (E-H) and anatomical (I-N) images obtained in the middle of the lateral tibial condyle at four different flexion angles. a) femur; b) tibia; c) lateral fabella; e) fibula; l) cranial horn of the lateral meniscus; m) caudal horn of the lateral meniscus.

4.3 Image Analysis

All measurements made by the two different observers were recorded in tables (**Table 1, Table 2, Table 3, Table 4**).

OBSERVER 1 MRI			LIGAMENT		MENISCUS		CARTILAGE	
CASE #	FLEX °	PLANE	CR CRUCIATE	CD CRUCIATE	MED	LAT	FEMUR	TIBIA
1	85	sag	3	3	3	3	3	3
		dor	3	3	2	3	3	3
	110	sag	3	2	3	3	3	3
		dor	3	3	3	3	3	3
	135	sag	2	2	3	3	3	3
		dor	2	1	2	2	2	2
	160	sag	1	1	1	3	2	2
		dor	1	1	1	2	1	1
2	85	sag	2	2	3	3	3	3
		dor	3	3	2	2	3	3
	110	sag	2	1	3	3	3	3
		dor	2	2	3	3	3	3
	135	sag	2	2	3	3	3	3
		dor	2	2	1	2	2	2
	160	sag	2	1	2	2	2	2
		dor	1	2	1	2	1	1
3	85	sag	2	3	2	2	2	2
		dor	2	2	1	2	1	1
	110	sag	2	3	3	3	3	3
		dor	3	3	1	1	1	1
	135	sag	3	2	3	3	3	3
		dor	2	3	2	3	1	1
	160	sag	3	3	3	3	3	3
		dor	3	3	2	3	1	1
4	85	sag	3	3	3	3	3	3
		dor	2	2	3	3	3	3
	110	sag	2	2	3	3	3	3
		dor	3	2	3	3	3	3
	135	sag	2	2	3	3	3	3
		dor	2	3	3	3	3	3
	160	sag	2	2	3	3	3	3
		dor	2	1	3	3	2	2
5	85	sag	2	3	3	3	3	3
		dor	2	3	3	3	3	3
	110	sag	3	3	3	3	3	3
		dor	2	2	3	3	3	3
	135	sag	2	2	3	3	3	3
		dor	1	2	3	3	3	3
	160	sag	2	2	3	3	2	2
		dor	1	1	2	2	2	2
6	85	sag	3	3	3	3	3	3
		dor	1	2	3	3	3	3
	110	sag	3	3	3	3	3	3
		dor	2	3	3	3	3	3
	135	sag	2	2	3	3	3	3
		dor	2	1	2	3	2	2
	160	sag	1	2	3	3	2	2
		dor	1	1	2	2	2	2

Table 1 - MRI visualization scores for observer 1

| OBSERVER 2 | | | LIGAMENT | | MENISCUS | | CARTILAGE | |
| MRI | | | | | | | | |
CASE #	FLEX °	PLANE	CR CRUCIATE	CD CRUCIATE	MED	LAT	FEMUR	TIBIA
1	85	sag	3	3	3	3	3	3
		dor	3	3	3	3	3	3
	110	sag	3	3	3	3	3	3
		dor	3	3	3	3	3	3
	135	sag	3	3	3	3	3	3
		dor	2	3	3	3	3	3
	160	sag	3	3	3	3	3	3
		dor	2	3	3	3	3	3
2	85	sag	2	2	3	3	3	3
		dor	3	3	2	2	3	3
	110	sag	2	1	3	3	3	3
		dor	2	2	3	3	3	3
	135	sag	2	2	3	3	3	3
		dor	2	2	1	2	2	2
	160	sag	2	1	2	2	2	2
		dor	1	2	1	2	1	1
3	85	sag	3	3	3	3	0	0
		dor	3	3	3	3	0	9
	110	sag	3	3	3	3	0	0
		dor	2	2	3	3	0	0
	135	sag	3	3	3	3	2	2
		dor	2	2	3	3	1	1
	160	sag	3	3	3	3	1	1
		dor	3	3	3	3	0	0
4	85	sag	3	3	3	3	1	1
		dor	2	2	3	3	1	1
	110	sag	3	3	3	3	1	1
		dor	2	2	3	3	1	1
	135	sag	3	3	3	3	1	1
		dor	3	3	3	3	1	1
	160	sag	3	3	3	3	1	1
		dor	2	2	3	3	1	1
5	85	sag	3	3	3	3	2	2
		dor	2	2	3	3	2	2
	110	sag	3	3	3	3	2	2
		dor	2	2	3	3	3	3
	135	sag	2	3	3	3	2	2
		dor	2	2	3	3	2	2
	160	sag	2	2	3	3	2	2
		dor	2	2	3	3	2	2
6	85	sag	3	3	3	3	1	1
		dor	2	2	3	3	1	1
	110	sag	3	3	3	3	1	1
		dor	2	2	3	3	1	1
	135	sag	3	3	3	3	2	2
		dor	2	2	3	3	1	1
	160	sag	1	2	3	3	1	1
		dor	2	2	3	3	1	1

Table 2 - MRI visualization scores for observer 2

OBSERVER 1 CT			LIGAMENT		MENISCUS		CARTILAGE	
CASE #	FLEX °	PLANE	CR CRUCIATE	CD CRUCIATE	MED	LAT	FEMUR	TIBIA
1	85	sag	2	3	2	2	0	0
		dor	2	2	2	2	0	0
	110	sag	1	3	2	2	0	0
		dor	1	2	2	2	0	0
	135	sag	2	3	2	2	0	0
		dor	2	2	2	2	0	0
	160	sag	2	2	2	2	0	0
		dor	1	2	2	2	0	0
2	85	sag	2	2	2	2	0	0
		dor	2	1	2	2	0	0
	110	sag	2	1	2	2	0	0
		dor	2	2	2	2	0	0
	135	sag	2	1	2	2	0	0
		dor	1	1	2	2	0	0
	160	sag	1	0	1	2	0	0
		dor	1	0	1	2	0	0
3	85	sag	1	2	2	2	0	0
		dor	1	2	1	2	0	0
	110	sag	1	2	2	1	0	0
		dor	2	2	1	1	0	0
	135	sag	1	1	2	2	0	0
		dor	2	2	2	2	0	0
	160	sag	1	1	1	2	0	0
		dor	1	1	1	1	0	0
4	85	sag	2	3	3	2	0	0
		dor	2	2	2	2	0	0
	110	sag	2	3	3	2	0	0
		dor	3	2	2	2	0	0
	135	sag	1	2	3	2	0	0
		dor	2	1	3	2	0	0
	160	sag	1	1	3	2	0	0
		dor	1	2	3	3	0	0
5	85	sag	2	2	3	2	0	0
		dor	2	1	1	1	0	0
	110	sag	3	3	3	2	0	0
		dor	2	2	3	2	0	0
	135	sag	3	3	3	2	0	0
		dor	1	1	3	2	0	0
	160	sag	1	2	3	2	0	0
		dor	1	1	2	2	0	0
6	85	sag	2	2	2	2	0	0
		dor	1	1	1	1	0	0
	110	sag	2	3	3	2	0	0
		dor	2	1	2	2	0	0
	135	sag	2	3	3	2	0	0
		dor	1	1	2	2	0	0
	160	sag	1	1	3	2	0	0
		dor	2	2	2	2	0	0

Table 3 - CT visualization scores for observer 1

OBSERVER 2 CT			LIGAMENT		MENISCUS		CARTILAGE	
CASE #	FLEX °	PLANE	CR CRUCIATE	CD CRUCIATE	MED	LAT	FEMUR	TIBIA
1	85	sag	3	3	3	3	1	1
		dor	3	3	3	3	1	1
	110	sag	3	3	3	3	1	1
		dor	3	3	3	3	1	1
	135	sag	3	3	3	3	1	1
		dor	2	2	3	3	1	1
	160	sag	3	3	3	3	1	1
		dor	2	2	3	3	1	1
2	85	sag	2	2	3	3	0	0
		dor	1	1	2	2	0	0
	110	sag	1	1	2	2	0	0
		dor	1	1	1	1	0	0
	135	sag	1	1	2	2	0	0
		dor	1	1	2	2	0	0
	160	sag	1	1	1	1	0	0
		dor	1	1	1	1	0	0
3	85	sag	2	2	2	2	0	0
		dor	2	2	2	2	0	0
	110	sag	2	2	3	3	0	0
		dor	1	1	2	2	0	0
	135	sag	2	2	2	2	0	0
		dor	1	1	2	2	0	0
	160	sag	2	2	2	2	0	0
		dor	1	1	1	1	0	0
4	85	sag	3	3	3	3	0	0
		dor	2	2	3	3	0	0
	110	sag	3	3	3	3	0	0
		dor	2	2	3	3	0	0
	135	sag	2	2	3	3	0	0
		dor	2	2	3	3	0	0
	160	sag	1	3	3	3	0	0
		dor	1	1	2	2	0	0
5	85	sag	3	3	3	3	1	1
		dor	3	3	3	3	1	1
	110	sag	3	3	3	3	1	1
		dor	3	3	3	3	1	1
	135	sag	3	3	3	3	0	0
		dor	3	3	2	2	0	0
	160	sag	2	2	3	3	0	0
		dor	2	2	2	2	0	0
6	85	sag	3	3	3	3	0	0
		dor	2	2	3	3	0	0
	110	sag	3	3	3	3	0	0
		dor	2	2	3	3	0	3
	135	sag	3	3	3	3	0	0
		dor	2	2	3	3	0	0
	160	sag	2	2	3	3	0	0
		dor	2	3	3	3	0	0

Table 4 - CT visualization scores for observer 2

4.4 Statistical Analysis

The Mean ± SD of the visualization scores obtained for the examined structures in the four different flexion angle are presented in **Table 5** for MRI and in **Table 6** for CT. In MR images the higher score mean for the CrCL was obtained at 85° and 110° of flexion, for the CdCL at 85°, for the menisci and the cartilage, both femoral and tibial, at 110° of flexion. In CT images the higher score mean for the CrCL and the femoral cartilage was obtained at 85° and 110° of flexion, for the CdCL and the tibial cartilage at 110°, for the medial meniscus at 135° and for the lateral meniscus both at 85° and 135° of flexion.

ANGLE		CR_cruciate	CD_cruciate	MED_menisc	LAT_menisc	FEMUR	TIBIA
85	Mean	2,500	2,667	2,750	2,833	2,208	2,583
	SD	0,590	0,482	0,532	0,381	1,062	1,666
110	Mean	2,500	2,417	2,917	2,917	2,292	2,292
	SD	0,511	0,654	0,408	0,408	1,083	1,083
135	Mean	2,208	2,292	2,708	2,875	2,250	2,250
	SD	0,509	0,624	0,624	0,338	0,794	0,794
160	Mean	1,917	2,000	2,458	2,708	1,708	1,708
	SD	0,776	0,780	0,779	0,464	0,807	0,807
Total	Mean	2,281	2,344	2,708	2,833	2,115	2,208
	SD	0,644	0,678	0,614	0,402	0,961	1,169

Table 5 – MRI visualization scores means ± SD. CR_cruciate= cranial cruciate ligament, CD_cruciate= caudal cruciate ligament; MED_menisc= medial meniscus, LAT_menisc= lateral meniscus, FEMUR= femoral cartilage, TIBIA= tibial cartilage, SD= standard deviation

ANGLE		CR_cruciate	CD_cruciate	MED_menisc	LAT_menisc	FEMUR	TIBIA
85	Mean	2,083	2,167	2,333	2,292	0,167	0,167
	SD	0,654	0,702	0,702	0,624	0,381	0,381
110	Mean	2,083	2,208	2,458	2,250	0,167	0,292
	SD	0,776	0,779	0,658	0,676	0,381	0,690
135	Mean	1,875	1,917	2,500	2,292	0,083	0,083
	SD	0,741	0,830	0,511	0,464	0,282	0,282
160	Mean	1,417	1,583	2,125	2,125	0,083	0,083
	SD	0,584	0,830	0,850	0,680	0,282	0,282
Total	Mean	1,865	1,969	2,354	2,240	0,125	0,156
	SD	0,734	0,814	0,696	0,611	0,333	0,443

Table 6 - CT visualization scores means ± SD. CR_cruciate= cranial cruciate ligament, CD_cruciate= caudal cruciate ligament; MED_menisc= medial meniscus, LAT_menisc= lateral meniscus, FEMUR= femoral cartilage, TIBIA= tibial cartilage, SD= standard deviation

There were higher visualization scores on MRI vs. CT, with a statistically significant difference for every structure (p<0,05). The pairwise comparison between MRI and CT is presented in **Table 7**.

	Modality		mean diff	std error	P	Wald	
						Lower	Upper
CR_cruciate	CT	MRI	-,417[a]	0,186	0,025	-0,780	-0,053
	MRI	CT	,417[a]	0,186	0,025	0,053	0,780
CD_cruciate	CT	MRI	-,375[a]	0,180	0,037	-0,727	-0,023
	MRI	CT	,375[a]	0,180	0,037	0,023	0,727
MED_menisc	CT	MRI	-,354[a]	0,096	0,000	-0,543	-0,166
	MRI	CT	,354[a]	0,096	0,000	0,166	0,543
LAT_menisc	CT	MRI	-,594[a]	0,072	0,000	-0,734	-0,453
	MRI	CT	,594[a]	0,072	0,000	0,453	0,734
FEMUR	CT	MRI	-1,990[a]	0,169	0,000	-2,321	-1,659
	MRI	CT	1,990[a]	0,169	0,000	1,659	2,321
TIBIA	CT	MRI	-2,052[a]	0,117	0,000	-2,282	-1,822
	MRI	CT	2,052[a]	0,117	0,000	1,822	2,282

Table 7 – Pairwise comparison between MRI and CT. CR_cruciate= cranial cruciate ligament, CD_cruciate= caudal cruciate ligament; MED_menisc= medial meniscus, LAT_menisc= lateral meniscus, FEMUR= femoral cartilage, TIBIA= tibial cartilage, mean diff= mean difference, std error= standard error

The effect of the single different flexion angle on the visualization scores for every structure for MR images is reported in **Table 8**. The 135° and 160° degrees of flexion had a statistically significant influence on femoral (p=0,016) and tibial cartilage (p=0,016). For the rest there were no statistical significant differences (p>0,05).

ANGLE			CR_cruciate	CD_cruciate	MED_menisc	LAT_menisc	FEMUR	TIBIA
85	P		0,363	0,295	0,126	0,504	1,000	1,000
	Confidence interval 99%	Lower limit	0,351	0,283	0,118	0,491	1,000	1,000
		Upper limit	0,376	0,307	0,135	0,517	1,000	1,000
110	P		0,288	0,729	1,000	1,000	1,000	1,000
	Confidence interval 99%	Lower limit	0,277	0,717	1,000	1,000	1,000	1,000
		Upper limit	0,300	0,740	1,000	1,000	1,000	1,000
135	P		0,064	0,454	0,060	0,249	0,016	0,016
	Confidence interval 99%	Lower limit	0,058	0,441	0,054	0,238	0,012	0,012
		Upper limit	0,070	0,467	0,066	0,261	0,019	0,019
160	P		0,064	0,454	0,060	0,249	0,016	0,016
	Confidence interval 99%	Lower limit	0,058	0,441	0,054	0,238	0,012	0,012
		Upper limit	0,070	0,467	0,066	0,261	0,019	0,019

Table 8 - Non-parametric Wilcoxon signed-rank test to evaluate the effect of the flexion angle on the visualization score (for MRI). CR_cruciate= cranial cruciate ligament, CD_cruciate= caudal cruciate ligament; MED_menisc= medial meniscus, LAT_menisc= lateral meniscus, FEMUR= femoral cartilage, TIBIA= tibial cartilage

The pairwise comparison among the different flexion angles for MR images is illustrated in **Table 9**. For the CrCL there is statistically significant difference in the visualization scores between 85° and 135° (p=0,019), 85° and 160° (p=0,015), 110° and 135 (p=0,033), 110° and 160° (p=0,019). For the CdCL there is statistically significant difference in the visualization scores between 85° and 135° (p=0,004), 85° and 135° (p=0,000), 110 and 160 (p=0,023). For the medial meniscus there is statistically significant difference in the visualization scores between 85° and 110° (p=0,028), 110° and 160° (p=0,034). For the lateral meniscus there is a statistically significant difference only between 135° and 160° (p=0,028). For the femoral cartilage there is statistically significant difference between 85° and 160° (p=0.040), 110° and 160° (p=0.007), 135° and 160° (p=0,000). For the tibial cartilage there is statistically significant difference between 85° and 160° (p=0,000), 110° and 160° (p=0,007), 135° and 160° (p=0,000).

ANGLE		CR_cruciate	CD_cruciate	MED_menisc	LAT_menisc	FEMUR	TIBIA
		P	P	P	P	P	P
85	110	1,000	0,109	0,028	0,273	0,083	0,353
	135	0,019	0,004	0,737	0,649	0,827	0,069
	160	0,015	0,000	0,143	0,330	0,040	0,000
110	85	1,000	0,109	0,028	0,273	0,083	0,353
	135	0,033	0,518	0,194	0,737	0,795	0,795
	160	0,019	0,023	0,062	0,249	0,007	0,007
135	85	0,019	0,004	0,737	0,649	0,827	0,069
	110	0,033	0,518	0,194	0,737	0,795	0,795
	160	0,125	0,069	0,034	0,028	0,000	0,000
160	85	0,015	0,000	0,143	0,330	0,040	0,000
	110	0,019	0,023	0,062	0,249	0,007	0,007
	135	0,125	0,069	0,034	0,028	0,000	0,000

Table 9 – Angles Pairwise Comparison (for MRI). CR_cruciate= cranial cruciate ligament, CD_cruciate= caudal cruciate ligament; MED_menisc= medial meniscus, LAT_menisc= lateral meniscus, FEMUR= femoral cartilage, TIBIA= tibial cartilage

The effect of the single different flexion angle on the visualization scores of every structure for CT images is reported in **Table 10**. The 85° degrees of flexion had a statistically significant influence on CdCL (p=0,007). For the rest there were no statistical significant differences (p>0,05).

ANGLE			CR_cruciate	CD_cruciate	MED_menisc	LAT_menisc
85	P		0,124	0,007	0,061	0,245
	Confidence interval 99%	Lower limit	0,116	0,005	0,054	0,234
		Upper limit	0,133	0,009	0,067	0,256
110	P		0,685	0,062	0,065	0,491
	Confidence interval 99%	Lower limit	0,673	0,056	0,058	0,478
		Upper limit	0,697	0,068	0,071	0,503
135	P		0,228	0,055	0,498	1,000
	Confidence interval 99%	Lower limit	0,217	0,049	0,485	1,000
		Upper limit	0,239	0,061	0,511	1,000
160	P		0,626	0,770	0,068	0,383
	Confidence interval 99%	Lower limit	0,613	0,759	0,061	0,370
		Upper limit	0,638	0,781	0,074	0,395

Table 10 - Wilcoxon signed-rank test to evaluate the effect of the flexion angle on the visualization scores (for CT). CR_cruciate= cranial cruciate ligament, CD_cruciate= caudal cruciate ligament; MED_menisc= medial meniscus, LAT_menisc= lateral meniscus, FEMUR= femoral cartilage, TIBIA= tibial cartilage

The pairwise comparison among the different flexion angles for CT images is illustrated in **Table 11**. For the CrCL there is statistically significant difference in the visualization scores between 85° and 135° (p=0,023), 85° and 160° (p=0,000), 110° and 160° (p=0,002). For the CdCL there is statistically significant difference in the visualization scores between 85° and 160° (p=0,000), 110° and 135° (p= 0,001), 110° and 160 (p=0,000). For the medial meniscus there is statistically significant difference in the visualization scores between 110° and 160° (p=0,017), 135° and 160° (p=0,014). For the lateral meniscus there is a statistically significant difference only between 135° and 160° (p=0,014).

		CR_cruciate	CD_cruciate	MED_menisc	LAT_menisc
ANGLE		P	P	P	P
85	110	1,000	0,702	0,376	0,702
	135	0,023	0,109	0,083	1,000
	160	0,000	0,000	0,352	0,235
110	85	1,000	0,702	0,376	0,702
	135	0,093	0,001	0,552	0,552
	160	0,002	0,000	0,017	0,014
135	85	0,023	0,109	0,083	1,000
	110	0,093	0,001	0,552	0,552
	160	0,000	0,001	0,014	0,083
160	85	0,000	0,000	0,352	0,235
	110	0,002	0,000	0,017	0,014
	135	0,000	0,001	0,014	0,083

Table 11 - Angles Pairwise Comparison (for CT). CR_cruciate= cranial cruciate ligament, CD_cruciate= caudal cruciate ligament; MED_menisc= medial meniscus, LAT_menisc= lateral meniscus, FEMUR= femoral cartilage, TIBIA= tibial cartilage

The Mean ± SD of the visualization scores for every structure, considering the plane, are presented in **Table 12** for MRI and **Table 14** for CT. The values are higher for the sagittal plane for every structure, both in MR images and CT images. The pairwise comparison between the two planes is illustrated in **Table 13** for MRI and in **Table 15** for CT. There is a statistically significant difference between the two planes for every structure in both the modalities. There is only no statistical difference (p=0,26) for the CdCL in MR images.

Plane		CR_cruciate	CD_cruciate	MED_menisc	LAT_menisc	FEMUR	TIBIA
dor	Mean	2,104	2,229	2,521	2,729	1,938	2,125
	SD	0,627	0,660	0,743	0,494	0,998	1,393
sag	Mean	2,458	2,458	2,896	2,938	2,292	2,292
	SD	0,617	0,683	0,371	0,245	0,898	0,898
Total	Mean	2,281	2,344	2,708	2,833	2,115	2,208
	SD	0,644	0,678	0,614	0,402	0,961	1,169

Table 12 – MRI visualization scores means for dorsal and sagittal plane. CR_cruciate= cranial cruciate ligament, CD_cruciate= caudal cruciate ligament; MED_menisc= medial meniscus, LAT_menisc= lateral meniscus, FEMUR= femoral cartilage, TIBIA= tibial cartilage, SD= standard deviation, dor= dorsal plane, sag= sagittal plane

	Plane		mean diff	std error	P	Wald Lower	Wald Upper
CR_cruciate	dor	sag	-,354[a]	0,090	0,000	-0,531	-0,177
	sag	dor	,354[a]	0,090	0,000	0,177	0,531
CD_cruciate	dor	sag	-0,229	0,205	0,264	-0,631	0,173
	sag	dor	0,229	0,205	0,264	-0,173	0,631
MED_menisc	dor	sag	-,375[a]	0,138	0,007	-0,646	-0,104
	sag	dor	,375[a]	0,138	0,007	0,104	0,646
LAT_menisc	dor	sag	-,208[a]	0,064	0,001	-0,333	-0,084
	sag	dor	,208[a]	0,064	0,001	0,084	0,333
FEMUR	dor	sag	-,354[a]	0,160	0,027	-0,667	-0,041
	sag	dor	,354[a]	0,160	0,027	0,041	0,667
TIBIA	dor	sag	-,167[a]	0,082	0,041	-0,327	-0,007
	sag	dor	,167[a]	0,082	0,041	0,007	0,327

Table 13 – Pairwise Comparison to evaluate the effect of the plane on the visualization scores (for MRI). CR_cruciate= cranial cruciate ligament, CD_cruciate= caudal cruciate ligament; MED_menisc= medial meniscus, LAT_menisc= lateral meniscus, FEMUR= femoral cartilage, TIBIA= tibial cartilage, SD= standard deviation, dor= dorsal plane, sag= sagittal plane, mean diff= mean difference, std error= standard error

Plane		CR_cruciate	CD_cruciate	MED_menisc	LAT_menisc	FEMUR	TIBIA
dor	Mean	1,729	1,708	2,167	2,146	0,125	0,188
	SD	0,676	0,713	0,724	0,652	0,334	0,532
sag	Mean	2,000	2,229	2,542	2,333	0,125	0,125
	SD	0,772	0,831	0,617	0,559	0,334	0,334
Total	Mean	1,865	1,969	2,354	2,240	0,125	0,156
	SD	0,734	0,814	0,696	0,611	0,332	0,443

Table 14 - CT visualization scores means for dorsal and sagittal plane. CR_cruciate= cranial cruciate ligament, CD_cruciate= caudal cruciate ligament; MED_menisc= medial meniscus, LAT_menisc= lateral meniscus, FEMUR= femoral cartilage, TIBIA= tibial cartilage, SD= standard deviation, dor= dorsal plane, sag= sagittal plane

	Plane		mean diff	std error	P	Wald	
						Lower	Upper
CR_cruciate	dor	sag	-,271[a]	0,069	0,000	-0,405	-0,136
	sag	dor	,271[a]	0,069	0,000	0,136	0,405
CD_cruciate	dor	sag	-,521[a]	0,100	0,000	-0,716	-0,326
	sag	dor	,521[a]	0,100	0,000	0,326	0,716
MED_menisc	dor	sag	-,375[a]	0,083	0,000	-0,538	-0,212
	sag	dor	,375[a]	0,083	0,000	0,212	0,538
LAT_menisc	dor	sag	-,188[a]	0,064	0,004	-0,313	-0,062
	sag	dor	,188[a]	0,064	0,004	0,062	0,313

Table 15 - Pairwise Comparison to evaluate the effect of the plane on the visualization scores (for CT). CR_cruciate= cranial cruciate ligament, CD_cruciate= caudal cruciate ligament; MED_menisc= medial meniscus, LAT_menisc= lateral meniscus, FEMUR= femoral cartilage, TIBIA= tibial cartilage, SD= standard deviation, dor= dorsal plane, sag= sagittal plane, mean diff= mean difference, std error= standard error

The Mean ± SD of the visualization scores given by the two different observer are reported in **Table 16** for MRI and in **Table 18** for CT. The values of the first observer are statistically significant lower than the values of the observer 2, both in MRI (**Table 17**) and CT (**Table 19**).

	CR_cruciate 1	CD_cruciate 1	MED_menisc 1	LAT_menisc 1	FEMUR 1	TIBIA 1	CR_cruciate 2	CD_cruciate 2	MED_menisc 2	LAT_menisc 2	FEMUR 2	TIBIA 2
Mean	2,125	2,188	2,542	2,750	2,521	2,521	2,438	2,500	2,875	2,917	1,708	1,896
SD	0,672	0,734	0,713	0,484	0,714	0,714	0,580	0,583	0,444	0,279	1,010	1,433
SEM	0,097	0,106	0,103	0,070	0,103	0,103	0,084	0,084	0,064	0,040	0,146	0,207

Table 16 – MRI visualization scores means for each observer. 1= first observer, 2= second observer, CR_cruciate= cranial cruciate ligament, CD_cruciate= caudal cruciate ligament; MED_menisc= medial meniscus, LAT_menisc= lateral meniscus, FEMUR= femoral cartilage, TIBIA= tibial cartilage, SD= standard deviation, SEM= standard error of mean

	CR_cruciate 2 - CR_cruciate 1	CD_cruciate 2 - CD_cruciate 1	MED_menisc 2 - MED_menisc 1	LAT_menisc 2 - LAT_menisc 1	FEMUR 2 - FEMUR 1	TIBIA 2 - TIBIA 1
P	0,001	0,006	0,001	0,017	0,000	0,000
Confidence interval 99% Lower limit	0,000	0,004	0,000	0,014	0,000	0,000
Upper limit	0,002	0,008	0,001	0,020	0,000	0,001

Table 17 - Wilcoxon signed-rank test to evaluate the interobserver differences (for MRI).

	CR_cruciate 1	CD_cruciate 1	MED_menisc 1	LAT_menisc 1	FEMUR 1	TIBIA 1	CR_cruciate 2	CD_cruciate 2	CR_MED 2	LAT_menisc 2	FEMUR 2	TIBIA 2
Mean	1,625	1,771	2,146	1,917	0,000	0,000	2,104	2,167	2,563	2,563	0,250	0,313
SD	0,606	0,805	0,684	0,347	0,000	0,000	0,778	0,781	0,649	0,649	0,438	0,589
SEM	0,087	0,116	0,099	0,050	0,000	0,000	0,112	0,113	0,094	0,094	0,063	0,085

Table 18 - CT visualization scores means for each observer. 1= first observer, 2= second observer, CR_cruciate= cranial cruciate ligament, CD_cruciate= caudal cruciate ligament; MED_menisc= medial meniscus, LAT_menisc= lateral meniscus, FEMUR= femoral cartilage, TIBIA= tibial cartilage, SD= standard deviation, SEM= standard error of mean

	CR_cruciate 2 - CR_cruciate 1	CD_cruciate 2 - CD_cruciate 1	MED_menisc 2 - MED_menisc 1	LAT_menisc 2 - LAT_menisc 1
P	0,000	0,001	0,000	0,000
Confidence interval 99% Lower limit	0,000	0,000	0,000	0,000
Upper limit	0,001	0,002	0,001	0,000

Table 19 - Wilcoxon signed-rank test to evaluate the interobserver differences (for CT). 1= first observer, 2= second observer, CR_cruciate= cranial cruciate ligament, CD_cruciate= caudal cruciate ligament; MED_menisc= medial meniscus, LAT_menisc= lateral meniscus

The k value mean for MRI is 0,28 (CrCL= 0,37, CdCL= 0,31, medial meniscus= 0,33, lateral meniscus= 0,47, cartilage= 0,09). The k value mean for CT is 0,14 (CrCL= 0,06, CdCL= 0,27, medial meniscus= 0,22, lateral meniscus= 0,01). The k values are lower than 0.40 indicating a poor agreement between the two different observers.

CHAPTER 5

Discussion

5. Discussion

Magnetic resonance imaging (MRI) is currently one of the most effective diagnostic tools for assessment of joint disorders (Grainger et al., 2000). The major advantages of MRI are its excellent image resolution, superior soft tissue contrast, the possibility to image in multiple planes and use of a magnetic field rather than ionizing radiations. All of these features have made MRI the diagnostic modality of choice for traumatic, degenerative and inflammatory diseases of joints in people (Rubin et al., 2000). Moreover, it is also the only noninvasive modality that allows combined evaluation of articular cartilage, subchondral bone and soft tissue structures associated with the joint. For all these reasons MRI of the knee is reported to be the most common non-neurologic application in human medicine (Chan et al., 1994).

From the first description of MRI of the canine stifle in 1991 (Widmer et al., 1991), several studies have described the use of low- and high- field MRI for the detection of intraarticular lesions and for diagnostic investigation of stifle injuries and degenerative changes (Baird et al., 1998; Martig et al, 2006; Blond et al., 2008; D'Anjou et al., 2008). Low-field systems are more common in veterinary practice, compared to high-field systems, because of their lower maintenance costs. However, low-field systems have disadvantages, because the signal-to-noise ratio, contrast and resolution increase with the field strength. Major disadvantage of low-field scanners is their poorer image resolution. It's more difficult to maintain the signal-to-noise ratio in a low-field system without increasing the slice thickness, the pixel sixe or the acquisition time. Lower resolution and increased slice thickness are likely to increase the partial volume effect, which could lead to a more difficult identification of small structures or lesions (Murray et al., 2009).

In a small body component like the stifle, the slice thickness and the imaging resolution during the imaging process are very important. The new multidetector CT scanners allow obtaining slices of sub-millimeters thickness. Helical CT has the potential to reduce the time of the examination considerably (Samii and Dyce, 2004) and CT images can be manipulated on the viewing console to demonstrate bone or soft tissue detail. Images can also be formatted into different image planes after acquisition. CT has been reported to be very sensitive in demonstrating calcified or bony structures and also allows evaluation of the soft-tissues using appropriate windows (Samii and Dyce, 2004; Soler et al.,

2007; Samii et al., 2009; Gielen et al., 2010). The osseous structures and the infrapatellar fat pad are clearly identifiable (Samii, 2011). Reformatting of the acquired transverse or frontal planar images is necessary to fully assess the cruciate and meniscal structures and intra-articular contrast medium is necessary to clearly see the intra-articular soft tissue structures (Samii, 2011).

Modern multidetector scanners allow the data to be reformatted as volumetric (3D) representations of structures and a 3D model can be constructed, displayed and manipulated for presurgical planning. Multislice CT allows very quick scanning of the patient and is a less expensive technique compared to MRI. For all these reasons, CT remains more widespread than MRI in veterinary practice.

The results from this study suggest that MRI is a valuable tool to adequately image the most clinical relevant components of the stifle joint and the stifle flexion angle affects the visualization of the most clinical relevant structures of the joint.

Scores obtained were significantly greater when using MRI compared to CT, as previously described (D'Anjou, 2008).

The most obvious difference comparing CT with MR images, was the greater soft-tissue contrast demonstrated in MR images. All the structures had a total visualization score > 2 with MRI; using CT the total values were significantly lower. Ligaments and menisci were seen in both modalities but clearly defined in the MR images, poorly demarcated in the CT images (Fig. 10, Fig. 11, Fig. 12).

Fig. 10 - Comparison between CT (A) and MRI (B) sagittal images at the level of the lateral meniscus.
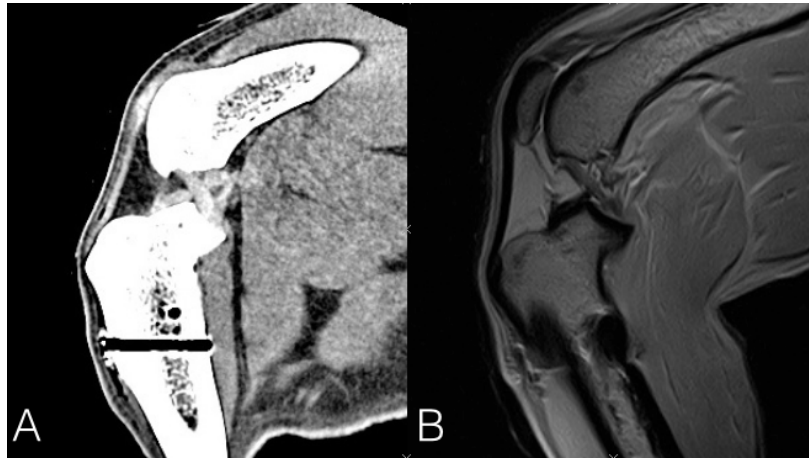
Fig. 11 - Comparison between CT (A) and MRI (B) sagittal images at the level of the intercondylar notch.
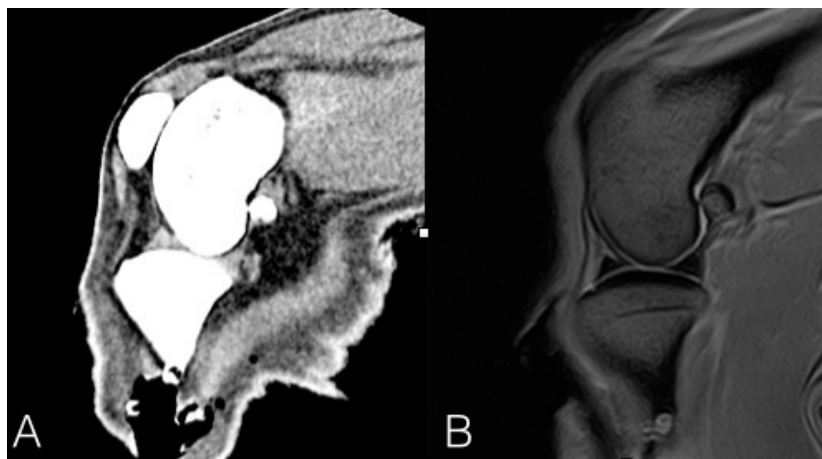
Fig. 12 - Comparison between CT (A) and MRI (B) sagittal images at the level of the medial meniscus.

The cartilage was difficulty identified in all the CT images and scored a total mean close to 0. For this reason we excluded it from some the statistical analysis. Also in MR images the scores obtained for the cartilage were not satisfactory. This is in agreement with previous human studies, which have shown that MR cannot replace direct visualization for diagnosing cartilage damage in the knee (Friemert et al., 2004; Von Engelhardt et al., 2007). A study from Galindo-Zamiro et al. (2013) concluded that the evaluation of the cartilage using MR is not clinically reliable in dogs. However, a recent study from Olive et al. (2010), performed to evaluate the metacarpophalangeal articular cartilage in horses, demonstrated that it is possible to evaluate cartilage thickness and structure using

a fat-suppressed spoiled gradient-recalled sequence. Thus, the use of other sequences could improve the visualization of the cartilage.

For MR imaging we choose to perform only a PD sequence, because our goal was to perform a morphological and comparative study.

A proton density image is one where the difference in the numbers of protons per unit volume in the patient is the main determining factor in forming image contrast. When an MRI sequence is set to produce a PD-weighted image, it's the tissue with the higher concentration or density of protons (hydrogen atoms), which produce the strongest signal and appears the brightest on the image.

The most used sequences in clinical practice are the T1 and T2 weighted images. PD weighted sequence produces contrast by minimizing the impact of T1 and T2 differences with long TR (2000-5000ms) and short TE (10-20). A long TR allows tissues e.g. fat and water to fully recover their longitudinal magnetization and therefore diminishes T1 weighting. A short TE does not give fat or water time to decay and therefore diminishes T2 weighting.

Our sequence was selected because it appeared to provide a good quality to properly image the normal anatomical structures. A study from Blond et al. (2008) about diagnostic accuracy of high-field MRI for meniscal tears in dogs affected with naturally occurring cranial cruciate ligament rupture reported a global sensitivity of 100% and specificity of 94% using proton density sequences. However, imaging of pathologic joints may require for sure more sophisticated sequences.

For CT images acquisition we used a soft tissue algorithm.

The advantage of the CT study was the time required for it. After positioning, each angle scan took only around 30 seconds, compared to the 30 minutes required for one MRI sequence.

There was a statistically significant ($p<0,05$) difference between the two observers. The interobserver agreement was poor both for CT and MRI (k<0.40). This is likely explained partially by the variable difference experience of examiners. The second observer had a longer working experience in radiology and in particular in the orthopedic field. The first observer is still at the beginning of the learning curve. The interobserver difference could be reduced having two same level trained radiologists. In addition, the scoring systems we used were qualitative and subjective. The use of a quantitative scoring system,

introducing appropriate measurements system of the target, could reduce the interobserver difference.

We performed the image analysis only comparing dorsal and sagittal plane. The transverse plane was not considered. Based on our experience and in accord with literature, all the structures are best identified working on these two planes (Blond et al., 2008; Pujol et al., 2011). They reported that dorsal and sagittal planes were most useful to identify structures like cruciate ligaments and menisci. From the results of our statistical analysis, scores obtained were statistically significantly greater ($p<0,05$) when comparing the sagittal to the dorsal plane, both in MRI and CT images (Fig. 13, Fig. 14).
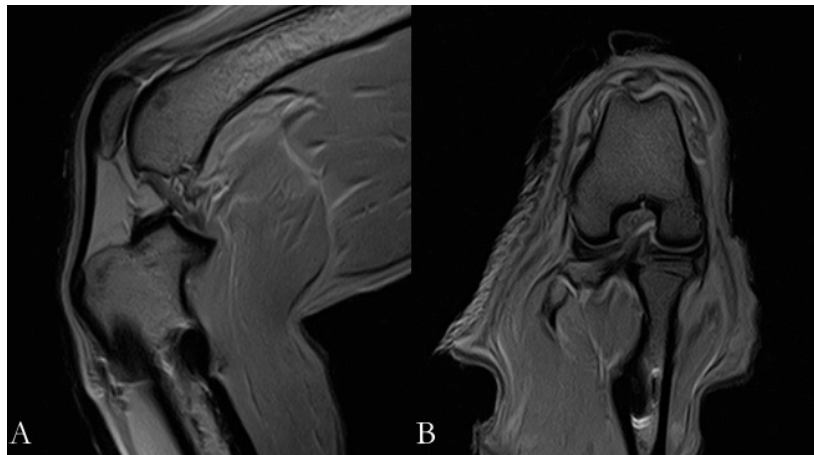
Fig. 13 - MRI images at the level of the intercondylar notch. Sagittal (A) and dorsal (B) planes.
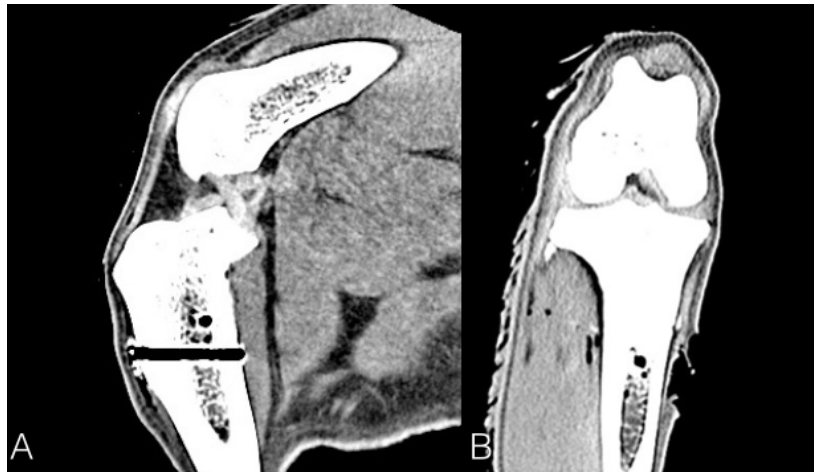
Fig.14 – CT images at the level of the intercondylar notch. Sagittal (A)
and dorsal (B) planes.

Visualization score were significatively affected by the stifle angle. From the
pairwise comparison between the different angle resulted that the best
visualization was obtained at 85° and 110° degree of flexion.

For the cranial cruciate ligament this may be related to its anatomical relation
with the surrounding structures. Similar to studies performed in people (Niitsu et
al., 1997), we observed that during extension the majority of the femoral portion
of the CrCL was in contact with the proximal and the lateral margins of the
intercondylar fossa and their contour couldn't be clearly delineated. During
flexion, the cranial cruciate ligament separated from this bony structures,
allowing synovial fluid to extend around the margins so the ligament was better
delineated (Fig. 8).

Menisci were best visualized at 110° of flexion, seen as wedge-shaped structures
on sagittal plane. It is well-know that joint motion results also in motion of the
menisci. During flexion the menisci slides caudally on the tibial plateau.
However, the medial meniscus slides much less than the lateral because of its
attachment to the medial collateral ligament and joint capsule (Carpenter and
Cooper, 2000; Arnoczky, 2001). The caudal displacement of the lateral femoral
condyle on the tibia during flexion makes the caudal displacement of the lateral
meniscus even more pronounced and, in extreme flexion, it may protrude over
the edge of the tibial plateau. During extension both menisci slide cranially on
the tibial plateau and they are more compressed between it and the femoral
condyles (Fig. 7, Fig. 9).

The technique described in this study could not be used in clinical patients because it required bone tunnels in tibia. In humans, MRI tracking systems allow for automatic continuous adjustments of scan plane positions (Vandevenne et al. 2010). Other methods described in humans include use of anatomical landmarks such as collateral ligaments, tibial condyles, or the caudal aspect of the tibial plateau (Mastrokalos et al., 2005). We used a method that would allow exact alignment of the scan, to have an almost perfect repeatability between different scans and between the two modalities. Further work is for sure required to validate anatomic landmarks in the canine stifle joint for clinical application.

We used disarticulated limbs. However, the stifle angulation should not represent a problem in the patient positioning. Nevertheless, further studies will be required for clinical application in live dogs.

5.1 Conclusions

All of the joint structure of the canine stifle can be better identified and evaluated by MRI. Most of the soft tissue structures that were seen on MRI were also identified on CT images using a soft tissue window, but never with the definition that MRI offers.

Our hypothesis was confirmed and imaging of the stifle in flexion conditions (range from 85° and 110°) resulted in better visualization and delineation of the main stile joint structures, with particular focus on the cruciate ligaments and the menisci. Exact positioning was a crucial point of this study. The tibial tunnels we used cannot be obviously applied in clinical patients. Future studies will be needed to find repeatable anatomical landmarks, such as the caudal aspect of the lateral tibial condyle and the intercondylar eminences.

CHAPTER 6

Summary

6. Summary

Several new imaging modalities have been described for the evaluation of the canine stifle. However, to our knowledge, imaging of the stifle at varying degree of flexion has not been investigated. Our purpose was to compare high field magnetic resonance (MRI) and computed tomography (CT) of the normal stifle at varying flexion angles to describe and evaluate the visualization of its structures when positioned in four different flexion angles (85°-110°-135°-160°). Six canine hind limbs were imaged at four different flexion angles using a 1.5 Tesla commercial MR unit and a multi-slices CT scanner. For each CT and MRI scan two board certified veterinary radiologists independently evaluated the cranial and the caudal cruciate ligament, the medial and the lateral meniscus, the femoral and tibial cartilage, using a visual assessment score of 0-3 and subjective criteria previously described by Podadera et al. A score of 0 indicated that the structure was not visible. A score of 1 indicated that the structure was visualized partially. A score of 2 indicated that the totality of the structure was identified but poorly demarcated. A score of 3 indicated that the structure was totally visualized and well demarcated. Statistical analysis was performed to evaluate the intermodality difference and the interobserver difference, the effect of each flexion angle and the effect of the plane on the visualization score of the different structures. The visualization scores obtained for MRI were statistically significant different compared to those obtained with CT images. There was statistically significant difference between the two observers. From the pairwise comparison of the different flexion angles the 85° and 110° degree of flexion resulted to be the best angles to visualize all the structures.

All of the joint structure of the canine stifle can be better identified and evaluated by MRI. Most of the soft tissue structures that were seen on MRI were also identified on CT images using a soft tissue window, but never with the definition that MRI offers.

Imaging of the stifle in flexion conditions resulted in better visualization and delineation of the main stile joint structures, with particular focus on the cruciate ligaments and the menisci.

7. References

Arnault, F., Cauvin, E., Viguier, E., Kraft, E., Sonet, J., Carozzo, C., 2009. Diagnostic value of ultra-sonography to assess stifle lesions in dogs after cranial cruciate ligament rupture: 13 case. Veterinary and Comparative Orthopaedics and Traumatology 22, 479-485

Arnoczky, S. P., Torzilli, P. A., Marshall, J. L., 1977. Evaluation of anerior cruciate ligament repair in the dog: An analysis of the instant center of motion. Journal of the American Animal Hospital Association 13, 553-558

Arnoczky, S. P., and Marshall, J. L., 1977. The cruciate ligaments of the canin stifle: an anatomical and functional analysis. American Journal of Veterinary Research 38, 1807-1812

Arnoczky, S. P., 1988. The cruciate ligaments: the enigma of the canine stifle. Journal of Small Animal Practice 29, 71-90

Arnoczky, S. P., 2001. Meccanica patologica dei trauma a carico dei legamenti crociati e dei menischi. In: Le Basi Patogenetiche delle Malattie Chirurgiche nei Piccoli Animali, M.J., Bojrab, Giraldi Editore, pp. 1023-1038

Arnoczky, S.P., 1993. Pathomechanics of cruciate ligament and meniscal injuries. In: Disease Mechanisms in Small Animal Surgery, M.J., Bojrab, ed, Philadelphia: Lea & Febiger, pp. 764-776

Baird, D.K., Hathcock, J.T., Rumph, P.F., Kincaid, S.A., Visco, D.M., 1998. Low-field magnetic resonance imaging of the canine stifle joint: normal anatomy. Veterinary Radiology & Ultrasound 39, 87-97

Baird, D.K., Hathcock, J.T., Kincaid, S. A., Rumph, P. F., Kammermann, J., Widmer, W. R., Visco, D., Sweet, D., 1998. Low-field magnetic resonance imaging of early subchondral cyst-like lesions in induced cranial cruciate ligament deficient dogs. Veterinary Radiology & Ultrasound 39, 167-173

Bellenger, C. R., 1995. Knee joint function, meniscal disease, and osteoarthritis. The Veterinary Quarterly 17, S5-S6

Barone, R., 2004. Anatomia comparata dei mammiferi domestici. Vol. 2°-parte I Artrologia, third ed., Edagricole, Bologna

Barrett, E., Barr, F., Owen M., Bradley, K., 2009. A retrospective study of the MRI findings in 18 dogs with stifle injuries. Journal of Small Animal Practice 50, 448-455

Blond, L., Thrall, D. E., Roe, S. C., Chailleux, N., Robertson, J. D., 2008. Diagnostic accuracy of magnetic resonance imaging for meniscal tears in dogs affected with naturally occurring cranial cruciate ligament rupture. Veterinary Radiology & Ultrasound 49, 425-431

Bottcher, P., Bruhschwein, A., Winkels, P., Werner, H., Ludewig, E., Grevel, V., Oechtering, G., 2010. Value of low-field magnetic resonance imaging in diagnosing meniscal tears in the canine stifle: a prospective study evaluating sensitivity and specificity in naturally occurring cranial cruciate ligament deficiency with arthroscopy as the gold standard. Veterinary Surgery 39, 296-305

Carpenter Jr, D. H., and Cooper, R. C., 2000. Mini review of canine stifle joint anatomy. Anatomia, Histologia, Embryologia 29, 321-329

Carrig, C. B., 1997. Diagnostic imaging of osteoarthritis. Veterinary Clinics of North America: Small Animal Practice 27, 777-814

Chan, W. P., Fritz, R. C., Steinbach, S. L., Wu, C. Y., et al., 1994. The knee: internal derangements. In MRI of the Musculoskeletal System, Chan, W. P., Lang, P., Genant, H. K., W B Saunders Co, Philadelphia, PA, pp. 263-306

D'Anjou, M. A., Moreau, M., Troncy, E., Martel-Pelletier, J. M., Abram, F., Raynauld, J., Pelletier, J., 2008. Osteophytosis, subchondral bone sclerosis, joint effusion and soft tissue thickening in canine experimental stifle osteoarthritis: comparison between 1.5t magnetic resonance imaging and computed radiography. Veterinary Surgery 37, 166-172

De Rooster, H., Van Ryssen, B., Van Bree, H., 1998. Diagnosis of cranial cruciate ligament injury in dogs by tibial compression radiography. Veterinary Record 142, 366-368

De Rooster, H., Van Bree, H., 1999. Use of compression stress radiography for the detection of partial tears of the canine cranial cruciate ligament. Journal of Small Animal Practice 40, 573-576

Evans, H. E., de Lahunta, A., 2013. Arthrology. In: Miller's Anatomy of the dog, Fourth ed. Saunders Elsevier, St. Louis, MO, USA, pp 177-181

Fitch, R. B., Wilson, E. R., Hatchcock, J. T. et al, 1997. Radiographic, computed tomographic and magnetic resonance imaging evaluation of a chronic long digital extensor tendon avulsion in a dog. Veterinary Radiology & Ultrasound 38, 177-181

Flo, G. L., 1993. Meniscal injuries. Veterinary Clinics of North America: Small Animal Practice 23, 831-843

Friemert, B., Oberlander, Y., Schwarz, W., Haberle, H. J., Bahren, W., Gerngross, H., Danz, B., 2004. Diagnosis of chondral lesions of the knee joint: can MRI replace arthroscopy? A prospective study. Knee Surgery, Sport Traumatology, Arthroscopy 12, 58-64

Galindo-Zamora, V., Dziallas, P., Ludwig, D. C., Nolte, I., Wefstaedt, P., 2013. Diagnostic accuracy of a short-duration 3 Tesla magnetic resonance protocol for diagnosing stifle joint lesions in dogs with non-traumatic cranial cruciate ligament rupture. BMC Veterinary Research 9, 40-48

Gielen I., Saunders, J., Van Ryssen, B., van Bree, H., 2010. Computed Tomography of the Stifle. In: Advances in The Canine Cranial Cruciate Ligament, Peter Muir, first ed., American College of Veterinary Surgeons Foundation and Wiley-Blackwell, 2010, pp 123-133

Gnudi, G., Bertoni, G., 2001. Echographic examination of the stifle joint affected by cranial cruciate ligament rupture in the dog. Veterinary Radiology & Ultrasound 42, 266-270

Grainger, A. J., Elliot, J. M., Campbell, R. S., Tirman, P. F., Steinbach, L. S., Genant, H. K., 2000. Direct MR arthrography: a review of current use. Clinical Radiology 55, 163-176

Hay, C. W., Aron, D. N., Roberts, R., Stallings, J., Brown, J., 1996. Evaluation of positive contrast arthrography in canine cruciate ligament disease. Veterinary and Comparative Orthopaedics and Traumatology 9, 10-13

Kippenes, H., Johnston, G., 1998. Diagnostic imaging of osteochondrosis. Veterinary Clinics of North America: Small Animal Practice 28, 137-160

Korvick, D. L., Pijanowski, G. J., Schaeffer, D. J., 1994. Three-dimensional kinematics of the intact and cranial cruciate ligament-deficient stifle of dogs. Journal of Biomechanics 27, 77-87

Kramer, M., Stengel H., Gerwing, M., Schimke, E., Sheppard, C., 1999. Sonography of the canine stifle. Veterinary Radiology & Ultrasound 40, 282-293

Leeson, T. S., Leeson, C. R., Paparo, A. A., 1988. Specialized connective tissue: cartilage and bone. In: Text/Atlas of Histology. Philadelphia: W.B. Saunders Company, pp. 159-194

Marino, D. J., Loughin, C. A., 2010. Diagnostic imaging of the canine stifle joint: a review. Veterinary Surgery 39, 284-295

Martig, S., Konar, M., Schmokel, H.G., Rytz, U., Spreg, D., Scheidegger, J., Hohl, B., Kircher, P.R., Boisclar, J., Lang, J., 2006. Low-field MRI and arthroscopy of meniscal lesions in ten dogs with experimentally induced cranial cruciate ligament insufficiency. Veterinary Radiology & Ultrasound 47, 515-522

Mastrokalos, D. S., Papagelopoulos, P. J., Mavrogenis, A. F., Hantes, M. E., Karachalios, T. S., Paessler, H. H., 2005. Changes of meniscal interhorn distances: an in vivo magnetic resonance imaging study. The Knee 12, 441-446

Messner, K., Gao, J., 1998. The menisci of the knee joint. Anatomical and functional characteristics, and a rationale for clinical treatment. Journal of Anatomy 193, 161-178

Metelman, L. A., Schwarz, P .D., Salman, M., Alvis, M. R., 1995. An evaluation of three different cranial cruciate ligament surgical stabilization procedures as they relate to postoperative meniscal injuries: a retrospective study of 655 stifles. Veterinary and Comparative Orthopaedics and Traumatology 8, 118-123

Mostafa, A. A., Griffon, D. J., Thomas, M. W., Constable, P. D., 2009. Morphometric characteristics of the pelvic limbs of Labrador Retriever with and without cranial cruciate ligament deficiency. American Journal of Veterinary Research 70, 498-507

Murray, R. C., Mair, T. S., Sherlock, C. E., Blunden, A. S., 2009. Comparison of high-field and low-field magnetic resonance images of cadaver limbs of horses. Veterinary Record 165, 281-288

Niitsu, M., Ikeda, K., Fukubayashi, T., Anno, I., Itai, Y., 1996. Knee extension and flexion: MR delineation of normal and torn anterior cruciate ligaments. Journal of Computer Assisted Tomography 20, 322-327

Niitsu, M., Ikeda, K., Itai, K., 1998. Slightly flexed knee position within a standard knee coil: MR delineation of the anterior cruciate ligament. European Radiology 8, 113-115

Olive, J., D'Anjou, M.A., Girard, C., Laverty, S., Theoret, C., 2010. Fat-suppressed spoiled gradient-recalled imaging of equine metacarpophalangeal articular cartilage. Veterinary radiology & Ultrasound 51, 107-115

Pozzi, A., Hildreth, B. E., Rajala-Schultz, P. J., 2008. Comparison of arthroscopiy and arthrotomy for diagnosis of medial meniscal pathology: an ex vivo study. Veterinary Surgery 37, 749-755

Pujol, E., Van Bree, H., Cauzinille, L., Poncet, C., Gielen, I., Bouvy, B., 2011. Anatomic study of the canine stifle using low-field magnetic resonance imaging (MRI) and MRI arthrography. Veterinary Surgery 4, 395-401

Reed, A. L., Payne, J. T., Constantinescu, G. M., 1995. Ultrasonography anatomy of the normal canine stifle. Veterinary Radiology & Ultrasound 36, 315-321

Robins, G. M., 1990. The canine stifle joint. In: Canine Orthopedics, Philadelphia: Lea & Febiger, pp. 693-702

Rubin, D. A., Paletta, G. A. Jr, 2000. Current concepts and controversies in meniscal imaging. Magnetic Resonance Imaging Clinics of North America 8, 243-270

Samii, V. F., Dyce, J., 2004. Computed tomographic arthrography of the normal canine stifle. Veterinary Radiology & Ultrasound 45, 402-406

Samii, V.F., Dyce, J., Pozzi, A., Drost, W., Mattoon, J.S., Green, E.M., Kowalesky, M.P., Lehman, A.M., 2009. Computed tomography arthrography of the stifle for detection of cranial and caudal cruciate ligament and meniscal tears in dogs. Veterinary Radiology & Ultrasound 50, 144-150

Samii, V. F., Gielen, I., Ludewig, E., Adams, W. H., Kiefer, I., van Bree, H., Saunders, J., 2011. Joints. In: Veterinary Computed Tomography. Schwarz, T. & Saunders, J., First Ed., John Wiley & sons Ltd, Southern Gate, Chichester, West Sussex, UK, pp. 387-419

Soler M., Murciano J., Latorre, R., Belda, E., Rodriguez, M.J., Agut A., 2007. Ultrasonographic, computed tomography and magnetic resonance imaging anatomy of the normal canine stifle joint. The Veterinary Journal 174, 351-361

Thrall, D. E., 2013. Textbook of Veterinary Diagnostic Radiology, 6th Ed. Saunders Elsevier, St. Louis, MO, USA

Tomlinson, J., 2005. Arthroscopy in the dog – what can be done? Small animal and exotics. Proceedings of the North America Veterinary Conference, 19, pp. 799-801. Orlando, Florida, USA, 8-12 January 2005

Tremolada, G., Winter, M. D., Kim, S. E., Spreng, D., Pozzi, A., 2014. Validation of stress magnetic resonance imaging of the canine stifle with and without an intact cranial cruciate ligament. American Journal of Veterinary Research 75, 41-47

Vandevenne, J., Pearle, A., Lang, P., Pauly, K. B., Bergman, G., 2010. Clinical feasibility of a magnetic resonance tracking system to guide the position of the scan plane during physiologic joint motion. La Radiologia Medica 115, 133-140

Vasseur, P. B., Arnoczky, S. P., 1981. Collateral ligaments of the canine stifle joint: anatomical and functional analysis. American Journal of Veterinary Research 42, 1133-1137

Von Engelhardt, L. V., Kraft, C. N., Pennekamp, P. H., Schild, H. H., Schmitz, A., von Falkenhausen, M., 2007. The evaluation of articulare cartilage lesions of the knee with a 3-Tesla magnet. Arthroscopy 23, 496-502

Widmer, W. R., Buckwalter, K. A., Braunstein, E. M., Visco, D. M., O'Connor, B. L., 1991. Principles of magnetic resonance imaging and application to the stifle joint in dogs. Journal of the American Veterinary Medical Association 198, 1914–1922

Widmer, W. R., Buckwalter, K. A., Braunstein, E. M., et al., 1994. Radiographic and magnetic resonance imaging of the stifle joint in experimental osteoarthritis of dogs. Veterinary Radiology & Ultrasound 35, 371-383

Winegardner, K. R., Scrivani, P. V., Krotscheck, U., Todhunter, R., 2007. Magnetic Resonance Imaging of subarticular bone marrow lesions in dogs with stifle lameness. Veterinary Radiology & Ultrasound 48, 312-317

8. Acknowledgements